APPROVED FOR RELEASE: 2007/02/08: CIA-RDP82-00850R000100010033-3

JPRS L/8226

17 January 1979

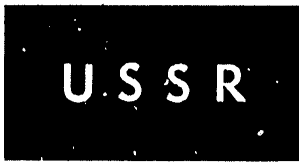

SELECTED TRANSLATIONS FROM THE SOVIET JOURNAL OF THE OPTICAL ENGINEERING INDUSTRY

U. S. JOINT PUBLICATIONS RESEARCH SERVICE

NOTE

JPRS publications contain information primarily from foreign newspapers, periodicals and books, but also from news agency transmissions and broadcasts. Materials from foreign-language sources are translated; those from English-language sources are transcribed or reprinted, with the original phrasing and other characteristics retained.

Headlines, editorial reports, and material enclosed in brackets [] are supplied by JPRS. Processing indicators such as [Text] or [Excerpt] in the first line of each item, or following the last line of a brief, indicate how the original information was processed. Where no processing indicator is given, the information was summarized or extracted.

Unfamiliar names rendered phonetically or transliterated are enclosed in parentheses. Words or names preceded by a question mark and enclosed in parentheses were not clear in the original but have been supplied as appropriate in context. Other unattributed parenthetical notes within the body of an item originate with the source. Times within items are as given by source.

The contents of this publication in no way represent the policies, views or attitudes of the U.S. Government.

PROCUREMENT OF PUBLICATIONS

JPRS publications may be ordered from the National Technical Information Service, Springfield, Virginia 22151. In ordering, it is recommended that the JPRS number, title, date and author, if applicable, of publication be cited.

Current JPRS publications are announced in Government Reports Announcements issued semi-monthly by the National Technical Information Service, and are listed in the Monthly Catalog of U.S. Government Publications issued by the Superintendent of Documents, U.S. Government Printing Office, Washington, D.C. 20402.

Indexes to this report (by keyword, author, personal names, title and series) are available through Bell & Howell, Old Mansfield Road, Wooster, Ohio, 44691.

Correspondence pertaining to matters other than procurement may be addressed to Joint Publications Research Service, 1000 North Glebe Road, Arlington, Virginia 22201.

APPROVED FOR RELEASE: 2007/02/08: CIA-RDP82-00850R000100010033-3

50272-101

REPORT DOCUMENTATION PAGE	1. REPORT NO. JPRS L/8226	2.	3. Recipient's Accession No.
4. Title and Subtitle: SELECTED TRANSLATIONS FROM THE SOVIET JOURNAL OF THE OPTICAL ENGINEERING INDUSTRY			5. Report Date: 17 January 1979 6.
7. Author(s)			8. Performing Organization Rept. No.
9. Performing Organization Name and Address: Joint Publications Research Service 1000 North Glebe Road Arlington, Va. 22201			10. Project/Task/Work Unit No. 11. Contract(C) or Grant(G) No. (C) (G)
12. Sponsoring Organization Name and Address: As above			13. Type of Report & Period Covered 14.

15. Supplementary Notes: OPTIKO-MEKHANICHESKAYA PROMYSHLENNOST', Leningrad, 1978

16. Abstract (Limit: 200 words)

This report contains a selection of articles on optical information processing systems, electrooptical direction-finding equipment and electrooptical scanning systems, and photodetectors. Several articles are devoted to characteristics of various types of optical glass.

17. Document Analysis a. Descriptors

USSR	Direction finding	Interferogram
Optics	Scanning	Optical glass
Information processing	Photodetectors	Dielectric mirrors

b. Identifiers/Open-Ended Terms

c. COSATI Field/Group 17B, 17C, 17H, 20F

18. Availability Statement	19. Security Class (This Report)	21. No. of Pages
FOR OFFICIAL USE ONLY. Limited number of copies available from JPRS	Unclassified	85
	20. Security Class (This Page) Unclassified	22. Price

(See ANSI-Z39.18) See Instructions on Reverse OPTIONAL FORM 272 (4-77) (Formerly NTIS-35) Department of Commerce

JPRS L/8226

17 January 1979

SELECTED TRANSLATIONS FROM THE SOVIET JOURNAL OF THE OPTICAL ENGINEERING INDUSTRY

Leningrad OPTIKO-MEKHANICHESKAYA PROMYSHLENNOST' in Russian 1978 No 8 pp 5-9, 17-23, 42-44, 59-61 and No 9 pp 7-10, 25-28, 36-42, 46-47, 56-58, 71-73

CONTENTS PAGE

CONTENTS (Continued) Page

PUBLICATION DATA

English title	:	SELECTED TRANSLATIONS FROM THE SOVIET JOURNAL OF THE OPTICAL ENGINEERING INDUSTRY
Russian title	:	OPTIKO-MEKHANICHESKAYA PROMYSHLENNOST'
Author (s)	:	
Editor (s)	:	
Publishing House	:	Optiko-Mekhanicheskaya Promyshlennost'
Place of Publication	:	Leningrad
Date of Publication	:	1978
Signed to press	:	
Copies	:	
COPYRIGHT	:	Optiko-Mekhanicheskaya Promyshlennost', 1978

APPROVED FOR RELEASE: 2007/02/08: CIA-RDP82-00850R000100010033-3

THE RELATION BETWEEN PARAMETERS OF AN OPTICAL INFORMATION PROCESSING SYSTEM AND CHARACTERISTICS OF THE OPTICAL ELEMENTS

Leningrad OPTIKO-MEKHANICHESKAYA PROMYSHLENNOST' in Russian
No 8, 1978 pp 5-7

[Article by L. I. Akopov, A. A. Ayazyan, V. Yu. Fedorov, and Ye. G. Tsitsishvili; all figures missing in original]

[Text] The relation is defined between the frequency contrast characteristic of an optical system and the basic parameters of an optical information processing system: volume of information, speed of operation, and reliability, which are determined by the density of information channels and the output power ratio between "one" and "zero" signals.

Recently in the development of computer equipment a great deal of attention has been given to the creation of systems for reading, writing, and transmitting discrete optical information in pictures (large blocks) consisting of combinations of light ("one") and dark ("zero") points [1-4]. Therefore it is necessary to evaluate optical elements in order to determine the possibilities for using them in computer systems. The most important characteristics of these systems are volume of information, speed of operation, and reliability. These parameters are interrelated, since the operational reliability at low signal levels is determined by the ratio of the energy of the "one" signal, I_1, to the energy of the "zero" signal, I_0, at the system output, and the value of these energies is related to the dimensions of the information points, the light flux density (luminance or illumination) on them, and the time the signal is present at the photodetector.

However, optical image transmission systems are characterized most fully by the frequency contrast characteristic (fcc) [5-8], which is essentially the coefficient of image contrast transmission as a function of the spatial frequency.

The light intensity distribution in the image plane i(x,y) is defined by the expression [6,7]

$$i(x, y) = \int_{-\infty}^{+\infty}\int O(\xi, \zeta)\, S(x-\xi, y-\zeta)\, d\xi d\zeta, \qquad (1)$$

where $O(\xi, \zeta)$ is the light intensity distribution in the object plane (the information picture); $S(x-\xi, y-\zeta)$ is the "scattering function" describing the light distribution in the (x,y) plane produced by a point source in the object plane (ξ, ζ). It is assumed that the "scattering function" is independent of possible noise (such as flashes in the image plane and the dark background). Therefore, strictly speaking, the following results pertain to "passive" systems of this kind.

Clearly the most "critical" type of information picture is the case of a "zero" surrounded by "ones". In this case the light distribution in the object plane may be expressed as

$$O(\xi, \zeta) = O_p(\xi, \zeta) + (J_0 - J_1)\,\mathrm{rect}\left(\frac{2\xi}{a}\right)\mathrm{rect}\left(\frac{2\zeta}{a}\right), \qquad (2)$$

where $O_p(\xi, \zeta)$ is an infinite periodic function with basic period a (equal to one step in the information picture) having the form

$$O_p(\xi, \zeta) = \begin{cases} J_1 \text{ when } |\xi| < \frac{a}{4},\ |\zeta| < \frac{a}{4}, \\ J_0 \text{ when } |\xi| < \frac{a}{2},\ \frac{a}{4} < |\zeta| < \frac{a}{2}; \\ |\zeta| < \frac{a}{4},\ \frac{a}{4} < |\xi| < \frac{a}{2}. \end{cases}$$

Here J_1 and J_0 are respectively the intensities of a "one" and a "zero" in the information field.

Formula (2) is written with the assumption that the linear dimensions of the information picture are much greater than its step, a. Having obtained the Fourier transformation of functions $O(\xi, \zeta)$ and $S(x-\xi, y-\zeta)$, and noting that the transform of the function $S(x-\xi, y-\zeta)$ is the fcc $\tau(\omega_x, \omega_y)$, and integrating according to formula (1), we obtain

$$i(x, y) = \sum_{n, m=-\infty}^{\infty} D_{nm}\,\tau\left(\frac{m}{a}, \frac{n}{a}\right) e^{\frac{2\pi}{a} i (mx+ny)} - \frac{J_1 - J_0}{\pi^2}\int_{-\infty}^{\infty}\int d\omega_x d\omega_y \frac{\sin\frac{\pi}{2}\omega_x a \sin\frac{\pi}{2}\omega_y a}{\omega_x \omega_y} \times \times \tau(\omega_x, \omega_y)\, e^{2\pi i (\omega_x x - \omega_y y)}. \qquad (3)$$

As follows from (3), to find a clear form of the function i(x,y) it is necessary to know the analytic form of the fcc $\tau(\omega_x, \omega_y)$ or to perform the numerical calculation (along the specific fcc curve for each optical element). Examination of only the periodic part of expression (4) simplifies the problem considerably and makes it possible to obtain qualitative results as well. Under these conditions the information picture is a collection of all the "ones" between which appear nothing but "zeroes". Since for such an information picture the ratio I_1/I_0 is less than that of the real picture, it is clear that the results obtained in this case will be low.

The intensity distribution in the image plane will be of the following form:

$$i(x, y) = D_{00}\tau(0, 0) + 2\sum_{n=1}^{\infty} D_{n0}\tau\left(\frac{n}{a}, 0\right)\cos\frac{2\pi}{a}ny + 2\sum_{m=1}^{\infty} D_{m0}\tau\left(\frac{m}{a}, 0\right)\cos\frac{2\pi}{a}mx + 4\sum_{n,m>1}^{\infty} D_{nm}\tau \times \left(\frac{n}{a}, \frac{m}{a}\right)\cos\frac{2\pi}{a}my\cos\frac{2\pi}{a}nx,$$

where

$$D_{00} = \frac{3J_0 - J_1}{4}; \quad D_{n0} = \frac{J_1 - J_0}{n}\sin\frac{\pi}{2}n;$$
$$D_{nm} = \frac{J_1 - J_0}{\pi^2 mn}\sin\frac{\pi}{2}n\sin\frac{\pi}{2}m; \; n \neq 0, \; m \neq 0.$$

If the image transmission scale in the periodic picture case is taken to be one, then the energies of "one" and "zero" at the output of the system will be, respectively,

$$I_1 = \int_{-\frac{a}{4}}^{\frac{a}{4}}\int_{-\frac{a}{4}}^{\frac{a}{4}} i(x, y)\,dx\,dy,$$

and

$$I_0 = \int_{-\frac{a}{4}}^{\frac{a}{4}} dy \int_{\frac{a}{4}}^{\frac{3}{4}a} i(x, y)\,dx. \qquad (4)$$

Performing the integration, for the ratio I_1/I_0 we obtain

$$\frac{I_1}{I_0} = \frac{\left(3 + \frac{J_1}{J_0}\right)\tau(0) + \left(\frac{4}{\pi}\right)^2\left(\frac{J_1}{J_0} - 1\right)S_1 + \frac{1}{4}\left(\frac{4}{\pi}\right)^4\left(\frac{J_1}{J_0} - 1\right)S_2}{\left(3 + \frac{J_1}{J_0}\right)\tau(0) - \frac{1}{4}\left(\frac{4}{\pi}\right)^4\left(\frac{J_1}{J_0} - 1\right)S_2}, \qquad (5)$$

where

$$S_1 = \sum_{n>1}^{\infty} \tau\left(\frac{2n-1}{a}, 0\right) \frac{1}{(2n-1)^2}$$

$$S_2 = \sum_{n,m>1}^{\infty} \tau\left(\frac{2n-1}{a}, \frac{2m-1}{a}\right) \frac{1}{(2n-1)^2(2m-1)^2}.$$

It should be noted that in general the fcc is a two-dimensional function. However, in view of the fact that the optical elements used must be axisymmetric, but the image plane must coincide with the surface of the image of mean curvature, the fcc does not depend on the direction of the spatial frequency and

$$\tau\left(\frac{m}{a}, \frac{n}{a}\right) = \tau\left(\frac{\sqrt{n^2+m^2}}{a}\right).$$

Expression (5) with a known fcc makes it possible to construct the ratio I_1/I_0 as a function of the density of information channels. Thus, for example, the fcc's presented in fig. 2 (for $J_1/J_0=20$) represent the functions shown in fig. 3. Corresponding to these curves, for information densities of interest it is clear that $S_1 < 1.2\,\tau(0)$ (the series (4) with $n,m > 3$ quickly diverge), and $I_1/I_0 < 8$. From formula (5) it also follows that with sufficiently large values of J_1/J_0 (specifically, $J_1/J_0 \gg 3$), $I_1/I_0 < 13$. For a given value of the ratio I_1/I_0, formula (5) makes it possible to estimate the corresponding minimum value of $\tau_{min}(1/a)$, and consequently also the maximum possible operating density of information channels satisfying the required relation

$$\tau_{min}\left(\frac{1}{a}\right) \approx \left(\frac{4}{\pi}\right)^2 \frac{\left(\frac{I_1}{I_0}-1\right)\left(3+\frac{J_1}{J_0}\right)\tau(0)}{\left(\frac{J_1}{J_0}-1\right)\sum_{n>2}^{3}\frac{1}{(2n-1)^2} + \left(\frac{2}{\pi}\right)^2\left(\frac{I_1}{I_0}+1\right)\sum_{\substack{n,m>1\\ n-1,\ m\neq 1\\ m-1,\ n\neq 1}}^{3}\frac{1}{(2n-1)^2}\frac{1}{(2m-1)}}. \quad (6)$$

Thus, for example, for $J_1/J_0=20$ and $I_1/I_0=4$, $\tau_{min}(1/a)=0.62\,\tau(0)$.

As indicated, examination of a periodic picture gives a low result. At the same time, the largest value of $\tau(1/a)$ obtained in examination of this picture is greater than the value of $\tau_{op}(1/a)$, corresponding to the true value of the operating density of information channels. It follows that an approximate estimation of the operating density may be obtained from expression (6).

Thus examination of a periodic picture makes it possible to obtain relations from which one may determine, according to the fcc's of the optical elements, the operating density of information channels in an optical information processing system as a function of the required value of the ratio of energies of a "one" and a "zero", I_1/I_0.

However, it must be taken into account that I_1/I_0 is the ratio of mean optical signal levels, which are of course subject to fluctuations. The degree of these fluctuations decreases as the signal level increases; that is, in order to guarantee reliable operation of a read/write system it is necessary to maintain the signal level as the signal passes through the optical system. There are methods of determining both the degree of fluctuation of the signal levels of "1's" and "0's" passing successively through an optical system [9] and the optimum receiver threshold providing the minimum probability of signal detection error [10]. If n_{min} is the minimum number of light quanta providing a given probability of reliable system operation and Δt is the time the signal acts on the photodetector, then taking into account the fact that the signal power is $\Phi = \frac{E}{4N^2}$ (N is the number of information channels per unit area and E is the value of the density), we obtain

$$\frac{E\Delta t}{N^2} = 4h\frac{c}{\lambda}n_{min},$$

where $h\frac{c}{\lambda}$ is the energy of a light quantum with wavelength λ.

Thus in choosing the parameters of systems for converting and transmitting optical information it is necessary to take into account both the fcc (the determination of the density of information channels) and the indicated mutually limiting relation between the speed of operation and the light flux density of picture elements.

In conclusion the authors express their gratitude to M. Ye. Perel'man for his interest in the work and useful discussions.

References

1. Shigin A. G., Deryugin A. A., "Tsifrovyye vychislitel'nyye mashiny," Moscow, ENERGIYA, 1975. [Digital computers]
2. Kitovich V. V., "Magnitnyye i magnitno-opticheskiye operativnyye zapominayushchiye ustroystva," [Magnetic and magnetooptic operational memory units], Moscow, ENERGIYA, 1975.
3. Chzhan' Ti, Zuk D., TIIER, 1975, vol 63, no 8, p 137.
4. Mikaelyan A. L. et al., KVANTOVAYA ELEKTRONIKA, 1971, no 1, p. 79.
5. Perren F., USPEKHI FIZ. NAUK, 1962, vol. 18 no. 2, October, p. 307
6. Neyl E., "Vvedeniye v statisticheskuyu optiku," [Intro-

duction to statistical optics] Moscow, MIR, 1966.
7. Mareshal' A., Franson M., "Struktura opticheskogo izobrazheniya," [The structure of an optical image] Moscow, MIR, 1964.
8. Semenov, Ye. P., OPT.-MEKH. PROMYSH., 1967, no 1, p. 12.
9. "Kaskadnyye elektronno-opticheskiye preobrazovateli i ikh primeneniye," [Multistage image converters and their application], ed. by M. M. Butslov, Moscow, MIR, 1965.
10. Curran T. E., Ross M., PROC. OF THE IEEE, 1965, vol. 53 no. 11, p. 1769

Received by editors 1 June 1977.

9187
CSO: 8144/468

EVALUATION OF STAR SENSOR ERRORS IN ELECTROOPTICAL DIRECTION-FINDING INSTRUMENTS

Leningrad OPTIKO-MEKHANICHESKAYA PROMYSHLENNOST' in Russian
No 8, 1978 pp 8-9

[Article by V. D. Smirnov]

[Text] An analysis is made of the effect of primary star sensor errors on the accuracy of determination of the direction in space to the star tracked. Formulae are derived determining the instrumental errors of a generalized model of a three-axis star sensor based on a two-axis gyrostabilizer. An expression is obtained for determining the magnitude of the total rms error of the star sensor.

Astronomical equipment has found wide use in highly complex navigation systems [1]. The basic subassembly determining system accuracy is the star sensor, which may be implemented both in a television version (an astrotelevision system) and in an optical tracking version (an automatic optical star tracking system). An analysis of the effect of instrumental errors of the star sensor on the precision with which the coordinates of a star are determined is necessitated by increased requirements for precision in astronomical equipment used to correct navigation systems [2].

The effect of instrumental errors on the precision of determining a given direction in space is most conveniently investigated by the method of solving spatial problems which was proposed for application to angle-measuring instruments [3] and is based on the use of spherical trigonometry. As distinct from optical angle-measuring instruments, whose geometric schemes are most often implemented in the altazimuthal version, star sensors may be built in any of three versions: orthodromic (horizontal-cruciform), equatorial, and altazimuthal. The most widely used are the first and third versions.

Therefore it is appropriate to examine a generalized geometric model which combines the orthodromic and altazimuthal schemes. Chosen as the model is the five-axis system shown in the figure, including a three-axis star sensor and a two-axis gyrostabilizer. The measurement axes of this system are a-a, b-b, and l-l. Fixing one of the axes (a-a or b-b), one obtains the orthodromic or the altazimuthal version of the system. Axes c-c and d-d of the two-axis gyrostabilizer, the roll and pitch axes, stabilize the measurement axes of the system in space.

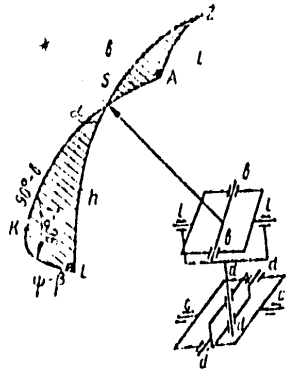

Geometric model of a five-axis system.

The relation of the altitude h and bearing angle β of the star to the angles b, l, and Ψ measured in the system is determined from the spherical triangle SAZ by the following equations:

$$\begin{aligned} \sin h &= \cos l \cos b, \\ \sin(\psi - \beta)\cos h &= \sin l \cos b, \\ \sin b &= \cos(\psi - \beta)\cos h. \end{aligned} \qquad (1)$$

The equations relating errors in altitude and bearing to errors with respect to the measurement axes may in the linear approximation be obtained by differentiating (1):

$$\begin{aligned} \Delta h &= -\Delta l \cos b \sin\alpha - \Delta b \cos\alpha, \\ \Delta\beta \cos h &= -\Delta l \cos b \cos\alpha + \Delta b \sin\alpha - \Delta\psi \cos h, \end{aligned} \qquad (2)$$

where Δl, Δb, and $\Delta\Psi$ are errors with respect to the measurement axes caused by faults in the manufacture and assembly of the system; α is the angle between arcs of the great circles [$\smile$(90°-b) and $\smile$h] in the right spherical triangle.

Errors in the determination of a given direction in space by the system may be suitably estimated by the magnitude of the ellipse of concentration on the celestial sphere with respect to the point whose direction is to be determined. The resulting magnitude of the ellipse is independent of which two axes (one of the measurement axes is unnecessary) the initial instrumental error was preliminarily assigned to. Therefore in further analysis of the given geometric model instrumental errors resulting from construction faults will be assigned to the b-b and l-l axes of the system.

Treating errors Δb, Δl, and $\Delta \Psi$ as random* and mutually uncorrelated, on the basis of the system of equations (2) it is simple to proceed to the rms errors of the system in altitude and bearing:

$$\sigma_h^2 = \sigma_l^2 \cos^2 b \sin^2 a + \sigma_b^2 \cos^2 a,$$
$$\sigma_\beta^2 \cos^2 h = \sigma_l^2 \cos^2 b \cos^2 a + \sigma_b^2 \sin^2 a. \quad (3)$$

The system of these equations determines the desired parameters of the ellipse of concentration of the point of intersection of the sighting line with the celestial sphere. From (3) we obtain a simple expression for determining the total rms error

$$\sigma^2 = \sigma_h^2 + \sigma_\beta^2 \cos^2 h = \sigma_l^2 \cos^2 b + \sigma_b^2. \quad (4)$$

The task of the following analysis is to determine the relation between the magnitudes of errors with respect to the measurement axes of the system (b-b and l-l) and the magnitudes of the initial faults producing these errors. Among initial faults in this case we include those faults in planning, assembling, and aligning the instrument which will, as the system rotates about its measurement axes, lead to a deviation of the optical axis from its intended trajectory in space. Included are non-orthogonality of the vertical axis of suspension a-a with the outer measurement axis l-l; non-orthogonality of the l-l axis with the inner measurement axis b-b; non-orthogonality of the optical axis of the system with the b-b suspension axis (collimation fault); and tilting of the vertical axis a-a.**

Instrumental error resulting from the fault of non-orthogonality of the a-a axis with the l-l axis is assigned to two axes and is expressed in the form

$$\Delta l = c_1 \operatorname{tg} b \sin l,$$
$$\Delta b_1 = c_1 (1 - \cos l), \quad (5)$$

---

*Errors Δb, Δl, and $\Delta \Psi$ result from a series of random faults in manufacture and assembly having a Gaussian distribution. Therefore they also are random and are characterized by the same distribution.

**Tilting of the a-a axis is a fault not of the star sensor but of the stabilizer and therefore will not be considered in the following. The effect of this fault on the measurement of altitude and bearing is determined by the well known relationships [1]:

$$\Delta h = -\Delta i \sin \beta + \Delta\theta \cos \beta \text{ и } \Delta\beta = \operatorname{tg} h (\Delta i \cos \beta + \Delta\theta \sin \beta),$$

where Δi and $\Delta \theta$ are compensation errors of the roll and pitch angles.

where c_1 is the magnitude of non-orthogonality of the axes.

Errors produced by the second fault (non-orthogonality of the 1-1 axis with the b-b axis) are assigned to only one axis (the error assigned to the second axis is negligible):

$$\Delta l_2 = c_2 \operatorname{tg} b, \tag{6}$$

where c_2 is the magnitude of non-orthogonality of the axes.

And finally the instrumental error resulting from collimation fault is also assigned to only one measurement axis:

$$\Delta l_3 = k\left(\frac{1}{\cos b} - 1\right), \tag{7}$$

where k is the collimation fault.

The formula for the total rms error produced by the faults examined above, based on the expressions in (4) and taking into account equations (5)-(7), assumes the form

$$\sigma = \left\{\sigma_k^2 (1 - \cos b)^2 + \sigma_{c_1}^2 [\sin^2 b \sin^2 l + (1 - \cos l)]^2 + \sigma_{c_2}^2 \sin^2 b\right\}^{1/2}, \tag{8}$$

where σ_k is the magnitude of the rms error of non-orthogonality of the optical axis with the inner suspension axis; σ_{c_1} is the magnitude of the rms error or non-orthogonality of the a-a axis with the 1-1 axis; and σ_{c_2} is the magnitude of the rms error of non-orthogonality of the inner suspension axis b-b with the outer axis 1-1.

It should be remarked that in optical angle-measuring instruments one of the manufacturing errors listed -- the collimation fault k -- is usually reduced by adjustment during the tuning-up process, and therefore its effect on the total rms error of the system is minimal (the magnitude of k does not exceed a few tenths of an arc minute).

The two remaining construction errors c_1 and c_2 are not eliminated in the tuning-up process because of the complexity of adjusting the suspension axes. As a result their magnitude is determined only by the technological precision of the manufacturing process and attains somewhat greater values (0.5-1.5') than the collimation error. Thus, taking into account the fact that the greatest contribution to the total error is made by the second and third terms in expression (8), this may be rewritten in the form

$$\sigma = \left\{\sigma_{c_1}^2 [\sin^2 b \sin^2 l + (1 - \cos l)^2] + \sigma_{c_2}^2 \sin^2 b\right\}^{1/2}. \tag{9}$$

Analysis of the formula obtained shows that errors in the generalized geometric star sensor model examined are minimal in the region near the zenith and increase as the sighting axis moves away from the zenith.

We will determine the specific value of the total rms error of the star sensor when it operates on the horizon; i. e., under conditions least favorable from the point of view of the accuracy characteristics of the angle-measuring instrument. In this case, when there is equality among the values appearing in the formula for the rms errors of non-orthogonality of the suspension axes ($\sigma_{c_1} = \sigma_{c_2} = \sigma_c$), we obtain

$$\sigma = \left\{ \sigma_c^2 [\sin^2 b \sin^2 l + (1 - \cos l)^2 + \sin^2 \delta] \right\}^{1/2} = 1{,}7\,\sigma_c,$$

that is, the value of the total rms error of the three-axis star sensor model examined, operating under the worst conditions, may vary within the limits

$$\sigma = 1.7(0.5\text{-}1.5') \approx 1'\text{-}2.5'.$$

Conclusions

1. Analysis of expression (8) shows that errors of the three-axis star sensor are minimal in the region near the zenith (with $\zeta = b = 0$) and increase as the optical axis moves away from the zenith. The greatest contribution to the total error is made by the second and third terms of the expression, characterizing the quality of the inner suspension axes.

2. When the initial errors appearing in expression (9) are equal, the total rms error of the three-axis geometric model $\sigma \approx 1{,}7\sigma_c$. In practice the values of errors of non-orthogonality of the axes may be reduced to $\sigma_c = 0.5\text{-}1.5'$, and as a result the total rms error of the three-axis system is $\sigma = 1.0\text{-}2.5'$.

References

1. Vorob'yev L. M., "Astronomicheskaya navigatsiya letatel'nykh apparatov," [Astronomical navigation of aircraft and spacecraft], Moscow, MASHINOSTROYENIYE, 1968.
2. O'Donnel K. F., "Inertsial'naya navigatsiya. Analiz i proyektirovaniye," [Inertial navigation. Analysis and planning], Moscow, NAUKA, 1969.
3. Pogarev G. V., "Yustirovka opticheskikh priborov," [Alignment of optical instruments], Leningrad, MASHINOSTROYENIYE, 1968.
4. Venttsel' Ye. S., "Teoriya veroyatnostey," [Probability theory], Moscow, FIZMATGIZ, 1962.

Received by editors 21 November 1977.

CONCURRENT OPTIMIZATION OF OPTICAL AND ELECTRICAL FILTERS IN SCANNING ELECTROOPTICAL SYSTEMS

Leningrad OPTIKO-MEKHANICHESKAYA PROMYSHLENNOST' in Russian
No 8, 1978 pp 17-20

[Article by Yu. N. Rakovskiy]

[Text] A method is proposed for concurrently optimizing the optical filters (of wavelengths of electromagnetic radiation) and electronic filters of a scanning electrooptical system taking into account internal noise and the interference of a nonuniform background.

We will examine a scanning electrooptical (eo) system whose output signal is formed by the relative displacement of an image of objects and the photodetector. The incoming optical signal is subjected in the eo system to both spectral filtering (of wavelengths of electromagnetic radiation) and (after conversion by the photodetector to an electrical signal) temporal filtering in an electronic amplification channel. Clearly the reaction of the system both to the useful signal and to the interference (background) is determined by the joint action of the optical and electronic filters.

This work is devoted to the problem of the optimum choice of the corresponding filters. Since in the scanning process there is a conversion from a spatial to a temporal signal, the electronic filter may be viewed as spatial, and the optimization of the eo system filters as spectral and spatial.

It will be useful to consider the signal from a point source, specified by its spectral irradiance at the input pupil of the objective lens of the eo system. Interference effects are internal system noise (basically, photodetector noise) and the external background, generally speaking a nonuniform luminance field. We will assume that the background is given either as

a finite set of spectral luminances of the various objects forming the background or as the spectral and spatial correlation function of the random luminance field as a whole. More detailed information on the background (higher order moments, multivariate distributions, and so on) is in general entirely lacking, and methods for practical use of it have thus far not been developed.

We will express the reaction of the eo system to the useful signal and the background interference by functionals of the optical filter $k(\lambda)$ (the light filter) and of the electronic filter, which will be described either by its transient response $h(t)$ or by its transfer function $K(\omega)$. One of the most important characteristics of the system is the output ratio of useful signal to internal noise. This parameter is easily monitored, and its comparison to the maximum possible (optimum for a given internal noise) value immediately shows the cost of achieving one or another degree of suppression of background interference. The signal-to-noise ratio at the output of a scanning eo system is

$$q = E \frac{\sqrt{2}\, S_0 \tau_0 D^*(\omega_\pi)\, k_c}{|K_{\pi\rho}(\omega_\pi)| \sqrt{S_{\pi\rho}\, \Delta f_ш}}. \qquad (1)$$

where E is the integral irradiance of the input pupil produced by radiation from a point source; S_0 is the area of the input pupil of the objective lens; τ_0 is the total transmittance coefficient of the objective lens (at the maximum of the spectral transmittance characteristic curve); $D^*(\omega_\pi)$ is the detection capability of the photodetector (at the maximum of its spectral response), measured at the frequency ω_π; $S_{\pi\rho}$ is the photosensitive surface area of the detector; $K(\omega)$ is the detector transfer function;

$$\Delta f_ш = \frac{1}{\pi} \int_0^\infty \frac{G(\omega)}{G(\omega_\pi)} |K(\omega)|^2 d\omega \qquad (2)$$

is the equivalent noise band of the eo system ($G(\omega)$ is the energy spectrum of photodetector noise);

$$k_c = \max_t |f_c(t) * h_{\pi\rho}(t) * h(t)| \qquad (3)$$

is the transmission coefficient of the pulse amplitude of the useful signal for the detector ($h_{\pi\rho}(t)$) and the filter ($h(t)$), while $f_c(t)$ is the form of the useful signal, which with constant scanning speed is the convolution of the scattering spot of the objective lens on the photosensitive area of the detector in the direction of scanning (in the time domain); and * is the operation of convolution.

Useful signals may be unequal both because of a difference in the objects themselves and because of variations in the conditions under which they are observed. If it is necessary to provide given output characteristics of the eo system for all possible signals, that is, even for the weakest, then it is natural to examine in the following form the integral irradiance of the input pupil appearing in (1):

$$E = \min_{\vec{l}} \int_{\Lambda} E(\lambda, \vec{l})\, k_{\text{опр}}(\lambda)\, k(\lambda)\, d\lambda, \qquad (4)$$

where $E(\lambda, \vec{l})$ is the spectral irradiance of the input pupil ($\vec{l}$ is the vector of parameters defining the various possible useful signals); $k_{\text{опр}}(\lambda)$ is the relative spectral response of the system consisting of optics and photodetector; $k(\lambda)$ is the desired filter; and Λ is the region over which the functions under the integral are defined.

It is convenient to introduce the normalized (with respect to signal amplitude and noise level) relation

$$\Psi = \frac{k_c}{k_{\text{ш}}} \quad (k_{\text{ш}} = \sqrt{\tau_0 \Delta f_{\text{ш}}}),$$

where $\tau_0 = a/v$ is the duration of the useful signal (a is the angular size of the photosensitive area of the detector in the direction of scanning; v is the speed of scanning), and the quantity

$$\frac{|K_{\text{пр}}(\omega_n)|}{S_0 \tau_0 D^*(\omega_n)} \sqrt{\frac{S_{\text{пр}}}{2\tau_0}} = \mathcal{E}. \qquad (5)$$

From (2) and (3) it follows that the quantity Ψ is the functional of the electronic filter, that is, $\Psi = \Psi\{h(t)\}$. The integral irradiance of the input pupil (4) is the functional of the filter $k(\lambda)$: $E = E\{k(\lambda)\}$. Therefore, taking into account the quantity (5), the output signal-to-noise ratio (1) may be re-written in the form

$$q = \frac{1}{\mathcal{E}} E\{k(\lambda)\}\, \Psi\{h(t)\}.$$

The maximum possible signal-to-noise ratio is

$$q_0 = \max_{k(\lambda),\, h(t)} q = \frac{1}{\mathcal{E}} \max_{k(\lambda)} E \max_{h(t)} \Psi = \frac{E_0 \Psi_0}{\mathcal{E}},$$

where

$$E_0 = E\{k(\lambda) = 1\}, \quad \Psi_0 = \Psi\{h_0(t)\},$$

and $h_0(t)$ is the transient response function of the electronic filter which maximizes the output signal-to-noise ratio. Normalizing

$$E\{k(\lambda)\}/E_0 = e\{k(\lambda)\}$$

and

$$\Psi\{h(t)\}/\Psi_0 = \psi\{h(t)\},$$

ultimately we obtain

$$q = q_0 e\{k(\lambda)\}\psi\{h(t)\}.$$

The normalized functionals e and Ψ directly define losses in the magnitude of the signal-to-noise ratio caused by measures taken to suppress background interference: the value $0 \leqslant e \leqslant 1$ defines losses resulting from limitation of the spectral band, and the value $0 \leqslant \Psi \leqslant 1$ defines those resulting from non-optimal (for a given internal noise) filtering in the electronic channel.

We will examine the reaction of the eo system to background interference. If, in addition to a set of spectral luminances of various background objects, there is no other information on the background, then background interference is usually treated as the response of the system to a drop (or jump) in luminance produced by the transition of the instantaneous field of view of the scanning system from one background object to another. The spectral luminances of the background objects may be either averaged over all possible conditions of observation or related to specific conditions. If it is necessary to provide a given quality of eo system operation in all (even the worst) background conditions, then the integral drop in luminance must be examined in the form

$$\Delta B = \Delta B\{k(\lambda)\} = \max_{i,j,\vec{g}} \left| \int_\lambda \left[B_i(\lambda, \vec{g}) - B_j(\lambda, \vec{g})\right] \times k_{опр}(\lambda) k(\lambda) d\lambda \right|, \quad (6)$$

where $\vec{g}$ is the vector of observation conditions and $B_i(\lambda,\vec{g})$ and $B_j(\lambda,\vec{g})$ are the spectral luminances of the ith and jth background objects, respectively.

The reaction of the eo system to a drop in luminance ΔB may conveniently be related, as with the useful signal, to the rms value of the internal noise; that is, the output signal-to-noise ratio may be considered to be

$$n = \frac{\Omega_{пр}\,\Delta B\{k(\lambda)\}}{\mathcal{G}} N\{h(t)\},$$

where $\Omega_{пр}$ is the solid angle of the photosensitive area of the detector (the instantaneous field of view), and the functional $N\{h(t)\}$ has the same meaning as $\Psi\{h(t)\}$, except that the form of the useful signal $f_c(t)$ in (3) must be replaced by the form of the interference $f_п(t)$:

$$N\{h(t)\} = \frac{k_п}{k_ш} = \frac{1}{k_ш} \max_t \left| f_п(t) * h_{пр}(t) * h(t) \right|,$$

where $f_п(t) = \int_0^t f_c(\tau) \frac{d\tau}{\tau_0}$ is the normalized response to a jump (the Heavyside function) without taking into account the detector inertia or the effect of the electronic filter. If the eo system were optimized only according to internal noise, then

the background-to-noise ratio would clearly be

$$n_0 = \frac{\Omega_{np}}{\mathcal{S}} \Delta B\{k(\lambda) = 1\} N\{h_0(t)\} = \frac{\Omega_{np}}{\mathcal{S}} \Delta B_0 N_0,$$

$$\Delta B_0 = \Delta B\{k(\lambda) = 1\}, \quad N_0 = N\{h_0(t)\}.$$

In the general case the background-to-noise ratio may be written in the form

$$n = n_0 b\{k(\lambda)\} \nu\{h(t)\}, \tag{7}$$

where

$$b\{k(\lambda)\} = \Delta B\{k(\lambda)\}/\Delta B_0;$$

and

$$\nu\{h(t)\} = N\{h(t)\}/N_0$$

are normalized functionals determining the degree of suppression of background interference by the methods of spectral and temporal filtering respectively.

The output signal-to-background ratio may be expressed similarly:

$$m = \frac{q}{n} = m_0 a\{k(\lambda)\} \varphi\{h(t)\}, \tag{8}$$

where

$$m_0 = \frac{E_0 \Phi_0}{\Omega_{np} \Delta B_0} \quad (\Phi_0 = \Phi_0'/N_0),$$

and

$$a\{k(\lambda)\} = \frac{e\{k(\lambda)\}}{b\{k(\lambda)\}},$$

$$\varphi\{h(t)\} = \frac{\psi\{h(t)\}}{\nu\{h(t)\}}.$$

For background having a given spectral and spatial correlation function of the random luminance field, we will also examine the background-to-noise and signal-to-background ratios, except that the response of the eo system to background interference will be characterized by the variance of the output signal from the background. We will derive an expression for the functionals corresponding to this case.

We will assume that at least approximately the spectral and spatial correlation function of the homogeneous (stationary in space) luminance field may be expressed in the form of a product

$$K(\lambda_1, \lambda_2, x, y) \approx B(\lambda_1, \lambda_2) R(x, y),$$

where R(x,y) is the correlation coefficient and $B(\lambda_1, \lambda_2)$ is the correlation function of spectral luminance, defining the variance of the integral luminance of the background in the following manner:

$$\sigma_B^2 = \int_{\Delta}\int_{\Delta} B(\lambda_1, \lambda_2) k_{onp}(\lambda_1) k_{onp}(\lambda_2) k(\lambda_1) k(\lambda_2) d\lambda_1 d\lambda_2. \tag{9}$$

The ratio of the rms values of background interference and internal noise at the output of the eo system is

$$n = \frac{\Omega_{\text{пр}}\sigma_B}{\mathcal{E}}\frac{k_\Phi}{k_{\text{ш}}} = \frac{\Omega_{\text{пр}}\sigma_B[k(\lambda)]}{\mathcal{E}}N[h(t)], \tag{10}$$

where

$$k_\Phi^2 = \frac{\Omega_\Phi}{\pi^2}\int_0^\infty\int_0^\infty \frac{G_B(\omega_x, \omega_y)}{G_B(0,0)}|K_{\text{опр}}(\omega_x, \omega_y)|^2 |K_{\text{пр}} \times (v\omega_x)K(v\omega_x)|^2 d\omega_x d\omega_y.$$

Here $K_{\text{опр}}(\omega_x, \omega_y)$ is the spatial and frequency response characteristic of the system consisting of the objective lens and the photodetector; $K_{\text{пр}}(v\omega_x)$ is the transfer function of the photodetector as an inertial element (the Fourier transformation of the function $h_{\text{пр}}(t)$); $K(v\omega_x)$ is the transfer function of the electronic filter (the Fourier transformation of the function h(t)); $G_B(\omega_x, \omega_y)$ is the Wiener spectrum of the integral luminance (the two-dimensional Fourier transformation of the spatial correlation function $\sigma_B^2 R(x, y)$);

$$\Omega_\Phi = \int_{-\infty}^{\infty}\int R(x, y)\,dx\,dy$$

is the background parameter, which for non-negative R(x,y) is the correlation region of the background (by analogy to the correlation interval for a one-dimensional process).

The background-to-noise ratio has the same form as in (7), but the functional $b[k(\lambda)]$ in this case is

$$b[k(\lambda)] = \frac{\sigma_B[k(\lambda)]}{\sigma_B[k(\lambda)\equiv 1]} = \frac{\sigma_B[k(\lambda)]}{\sigma_{B_0}},$$

where $\sigma_B[k(\lambda)]$ is determined by expression (9), and the functional of the electronic filter $v = N[h(t)]/N_0$ is determined by (10) since $N = k_\Phi/k_{\text{ш}}$. The same must be taken into account also in the signal-to-background ratio (8), where in this case $m_0 = E_0\Phi_0/\Omega_{\text{пр}}\sigma_{B_0}$.

Thus all necessary expressions have been determined for the output ratios of signal to noise q, background to noise n, and signal to background m both for the case when the background interference is treated in the form of a response of the eo system to a jump (or a drop) in luminance and for the case when the response of the eo system to the background is considered as a variance of the output background signal. Based on the expressions obtained, any criterion for the optimization of the filters may be formulated as a conditional or unconditional extremum problem:

$$\operatorname*{extr}_{k(\lambda),\,h(t)} F_1(q, n),$$

$$F_2(q, n) = C \quad \text{(conditional extremum)} \tag{11}$$

or

$$\operatorname*{extr}_{k(\lambda),\,h(t)} F(q, n) \quad \text{(unconditional extremum)} \qquad (12)$$

where $F(q,n)$ are given functions (the optimization criterion) of the functionals q and n; and C is a given constant. Examples of various criteria are

$$\max_{\substack{k(\lambda),\,h(t)\\ q\,\geqslant\,q_n}} \frac{q}{n}, \quad \max_{k(\lambda),\,h(t)} \frac{q^2}{n}, \quad \max_{k(\lambda),\,h(t)} (q - n), \quad \max_{k(\lambda),\,h(t)} \frac{q}{\sqrt{1+n^2}}$$

and so on.

The first of the listed criteria is most appropriate when the background is given only as characteristics of separate components of the objects and the background-to-noise ratio has the meaning of a response of the eo system to a drop in luminance between two different objects relative to the rms noise value. It is natural to use the last criterion when the background interference is evaluated as a variance since it represents the unconditional maximization of the ratio of the useful signal to the sum of the variances of the internal noise and the background interference. If additionally noise and background are time-independent Gaussian processes, then the eo system optimized according to this criterion will be optimal statistically as well (in the probabilistic sense).

We will show that problems (11) and (12) may be solved easily if we have all possible solutions to the problem

$$\min_{\substack{k(\lambda),\,h(t)\\ q\,\geqslant\,q_n}} (n), \qquad (13)$$

or the problem

$$\max_{\substack{k(\lambda),\,h(t)\\ n\,\leqslant\,n_n}} (q) \qquad (14)$$

that is, all possible pairs of filters $k^\circ(\lambda)$ and $h^\circ(t)$, each corresponding to a specific value of the threshold level $q_n \in [0, q_0]$ in problem (13) or $n_n \in [0, n_0]$ in problem (14). Since (13) and (14) are a dual problem pair [1, p 87], their solutions $n_{min}(q_n)$ and $q_{max}(n_n)$ are mutual inverse functions, and sets of optimum filters coincide if the limits q_π and n_π are varied through the entire range of their possible values. This property of a dual problem pair makes it possible to limit oneself to any one of them singly.

Let there be a complete solution to problem (13), that is, a function $n_{min}(q_n)$ and a set (practically speaking, of course, a finite collection) of pairs of filters $k^\circ(\lambda)$ and $k^\circ(t)$, each corresponding to a specific value of q_π from the interval $[0, q_0]$.

Based on the results of [2] we obtain

$$\operatorname*{extr}_{k(\lambda),\, h(t)} F_1(q, n) = \operatorname*{extr}_{q_\pi} F_1(q_\pi, n_{\min}(q_\pi)),$$

$$F_2(q, n) \leq C, \quad F_2(q_\pi, n_{\min}(q_\pi)) \leq C,$$

that is, the conditional extremum of the functional of functions $k(\lambda)$ and $h(t)$ is reduced to the determination of the extremum of a function of one variable q_π within a certain range defined by the condition $F_2(q_\pi, n_{\min}(q_\pi)) \leq C$. Similarly, problem (12) is reduced to the determination of the extremum of the function $F(q_\pi, n_{\min}(q_\pi))$ in the variable q_π over the entire range of possible values of this variable. According to the value of q_π° yielding the extremum of the functional F_1 (or F), we choose from the already determined set of filters $k^\circ(\lambda)$ and $h^\circ(t)$ the pair of filters which corresponds to this particular value of q_π°.

We will now show that the solution of problem (13) also in turn reduces to finding the extremum (minimum) of a function of one variable if all solutions are known to problems similar to (13) but related to each type of filtering (spectral and temporal) separately. In fact,

$$\min_{\substack{k(\lambda),\, h(t) \\ q \geq q_\pi}} (n) = n_0 \min_{\substack{k(\lambda),\, h(t) \\ e\{k(\lambda)\} \psi\{h(t)\} \geq q_\pi/q_0}} [b\{k(\lambda)\} \nu\{h(t)\}] = n_0 \min_{k(\lambda)} \left[b\{k(\lambda)\} \min_{\substack{h(t) \\ \psi\{h(t)\} \geq q_\pi/q_0 e\{k(\lambda)\}}} \nu\{h(t)\} \right] =$$

$$= n_0 \min_{k(\lambda)} \left[b\{k(\lambda)\} \nu_{\min}\left(\frac{q_\pi}{q_0 e\{k(\lambda)\}} \right) \right] = n_0 \min_{e_\pi} \left[b_{\min}(e_\pi) \nu_{\min}\left(\frac{q_\pi}{q_0 e_\pi} \right) \right],$$

where $b_{\min}(e_\pi)$ is the result of solving the conditional extremum problem for spectral filtering

$$\min_{\substack{k(\lambda) \\ e\{k(\lambda)\} \geq e_\pi}} b\{k(\lambda)\}$$

for all e_π from the interval [0,1] and $\nu_{\min}(\psi_\pi)$ is the solution to the conditional extremum problem for temporal filtering

$$\min_{\substack{h(t) \\ \psi\{h(t)\} \geq \psi_\pi}} \nu\{h(t)\}$$

for all ψ_π from the interval [0,1].

For optimization criteria formulated as an unconditional extremum (12), it is sometimes more convenient to represent the solution in the form of the extremum of a function of two variables:

$$\operatorname*{extr}_{k(\lambda),\, h(t)} F(q, n) = \operatorname*{extr}_{k(\lambda),\, h(t)} F(q_0 e\psi, n_0 b\nu) =$$

$$= \operatorname*{extr}_{e_\pi,\, \psi_\pi} F(q_0 e_\pi \psi_\pi, n_0 b_{\min}(e_\pi) \nu_{\min}(\psi_\pi)),$$

For example,

$$\max_{h(\lambda),\, h(t)} \frac{q}{\sqrt{1+n^2}} = q_0 \max_{e_n,\, \psi_n} \frac{e_n \psi_n}{\sqrt{1+n_0^2 b^2_{\min}(e_n)\, \nu^2_{\min}(\psi_n)}}.$$

We note also that any criterion F(q,n) may be replaced by $\Phi(q, m)$, where m=q/n is the signal-to-background ratio, and the "basic" problem instead of (13) becomes

$$\max_{\substack{h(\lambda),\, h(t) \\ q > q_0}} (m).$$

Thus for concurrent optimization of filters according to any criterion it is necessary to have all solutions to conditional extremum problems for spectral (15) and temporal (16) filtering separately. The remaining operations (determining the extremum of a function of one or two variables) are elementary.

Methods for solving spectral filtering extremum problems for functionals (4), (6), and (9) are examined in [3]. The conditional extremum problem for the filter h(t) in its general form is quite complex. However, in the practically important case in which the structure of the filter is given and only its parameters are to be determined, this problem is algorithmically simpler than the problem of spectral filtering. In this case it is necessary to specify a set (in practice a finite collection) of parameters of the filter, and by this a set of filters, and among them to find those which satisfy the conditions of the extremum problem. If all these filters are enumerated, then the problem itself (16) takes the form

$$\min_{\substack{i \\ \psi_i > \psi_0}} \nu_i \qquad (17)$$

where i=1, 2..., N is the filter number. The solution of problem (17) may be obtained, for example, using the following algorithm.

We will order the collection of all previously calculated values of Ψ so as to satisfy the strict inequalities

$$\psi_1 < \psi_2 < \ldots < \psi_M \ (M < N).$$

For this we will exclude all filters (except one) which reduce to equal values of Ψ, that is, in each group of such filters we will leave only the one which gives the smallest value of the quantity ν. (If in the group of filters corresponding to equal Ψ's there turn out to be several filters giving lowest but equal values of ν, then clearly it is possible to choose any one of them). Now, proceeding step by step from the end of the ordered sequence to its beginning (that is, beginning from the number M-1), we exclude from it all elements φ_i for

which $\nu_j > \nu_r$ where r is the number of the element left (that is, not excluded) at the previous step of this procedure. Then the remaining elements ψ_j and ν_j and the filters corresponding to them will be solutions to problem (17) at the points $\psi_0 = \psi_r$.

In conclusion we note that the proposed method for concurrently optimizing optical and electronic filters, based on the preliminary solution of problems for spectral (15) and temporal (16) filtering, has a number of advantages.

1. The solutions to problems (15) and (16) are "building blocks" which may be used to synthesize widely differing eo systems according to various criteria for optimization.

2. These solutions directly determine the effectiveness of that type of filtering, that is, they show what price (what reduction in the ratio of useful signal to noise) is paid for one or another degree of suppression of background interference.

3. If one of the filters is given and it is necessary to find the other one, then the method is easily simplified: if the filter $k(\lambda)$ is given, then

$$n_{\min} = n_0 b \nu_{\min}\left(\frac{q_n}{q_0 e}\right),$$

and if the filter h(t) is given, then

$$n_{\min} = n_0 \nu b_{\min}\left(\frac{q_n}{q_0 \tilde{\psi}}\right).$$

References

1. Gol'shteyn Ye. G., "Teoriya dvoystvennosti v matematicheskom programmirovanii i yeye prilozheniya," [Duality theory and applications in mathematical programming], Moscow, NAUKA, 1971.
2. Rakovskiy Yu. N., Smirnov A. P., OPT.-MEKH. PROMYSH., 1975, no. 2, pp. 14-15.
3. Rakovskiy Yu. N., OPT.-MEKH. PROMYSH., 1974, no. 11, pp. 16-17.

Received by editors 17 November 1977.

9187
CSO: 8144/468

ANALYSIS OF METHODS FOR TAKING INTO ACCOUNT RASTER DISTORTIONS AND INSTABILITIES IN ELECTROOPTICAL INSTRUMENTS WITH ELECTRONIC SCANNING

Leningrad OPTIKO-MEKHANICHESKAYA PROMYSHLENNOST' in Russian
No 8, 1978 pp 20-23

[Article by V. K. Sablin, V. A. Osipik, and V. I. Fedoseyev]

[Text] Examines the effect of distortions and instabilities on the electronic raster in electrooptical instruments with electronic scanning on the precision of measurement of coordinates of point targets. Relationships are derived determining measurement error for various calibration methods.

It is well known that electrooptical instruments with electronic scanning have, in addition to substantial favorable qualities, one drawback -- the occurrence of instabilities and distortions in the electronic raster. This article examines methods for taking into account these facts in relation to the measurement of coordinates of point targets and shows that with the appropriate choice of one or another method a high degree of measurement precision may be obtained.

General relationships

In an electrooptical instrument a two-dimensional image is converted into an electrical signal so that each point in the observed portion of space (the field of view) is assigned a pair of numbers determining the position of that point with respect to the electronic raster. These numbers will be called the raster coordinates and designated (t,T).

If a system of rectangular coordinates x, y is introduced in the object plane such that the x-axis is parallel to the direction of line scan in the center of the raster, and the coordinate center lies on the sighting axis of the instrument, then for each point in the object plane with coordinates (x,y) there will be a corresponding pair of raster coordinates (t,T).

Therefore we will consider that the instrument performs a mutually single-valued transformation of (x,y) coordinates onto (t,T) coordinates:

$$x = x(t, T), \quad y = y(t, T),$$
$$t_1 \leqslant t \leqslant t_2, \quad T_1 \leqslant T \leqslant T_2, \tag{1}$$

in which the functions x(t,T) and y(t,T) are sufficiently smooth. Because of the presence of raster distortions this transformation is nonlinear.

Measuring the coordinates of a point target requires that for values of (t,T) fixed by the instrument, the corresponding true (x,y) coordinates be determined.

If distortions and instabilities are not present, then the functions in (1) have the form

$$x(t, T) = x(t) = v_x(t - t_0),$$
$$y(t, T) = y(t) = v_y(T - T_0),$$

where (t_0,T_0) is the initial measuring point and v_x, v_y are known coefficients determining the scale of the transformation.

Further analysis will be performed only for x-coordinates; all relations are analogous for y-coordinates.

In the general case the functions in (1) may be written in the form of a Taylor series [1]

$$x(t, T) = x(t_0, T_0) + x'_t(t_0, T_0)(t - t_0) + x'_T(t_0, T_0)(T - T_0) + \frac{1}{2}\left[x''_{tt}(t_0, T_0)(t - t_0)^2 + 2x''_{tT}(t_0, T_0)(t - t_0)(T - T_0) + x''_{TT}(t_0, T_0)(T - T_0)^2\right] + \ldots$$

Reordering terms we obtain

$$x(t, T) = x(t_0, T_0) + x'_t(t_0, T_0)(t - t_0) + R(t - t_0) + \Delta x_r(t - t_0, T - T_0). \tag{3}$$

Here $R(t-t_0)$ represents the sum of terms containing only $(t-t_0)$ of degree 2 through ∞, and in the last component are included all terms containing $(T-T_0)$ in various degrees. The component $R(t-t_0)$ is associated with deflection nonlinearity along the scan line, and Δx_r is associated with geometric distortions. It is important to note that since in Δx_r there appear components containing the factor $(T-T_0)$ in various degrees, when $T=T_0$ we have $\Delta x_r = 0$.

Measurement without calibration

In measurement without calibration the relations in (1) obtain, that is, they are considered linear, having the form of (2) with known parameters t_0, T_0, v_x, and v_y. Subtracting (2) from (3), we obtain the absolute measurement error

$$\delta x = \delta x_0 + \delta v_{x0}(t - t_0) + R(t - t_0) + \\ + \Delta x_f(t - t_0,\ T - T_0).$$

where $\delta v_{x0} = x(t_0, T_0)$ is the error caused by uncertainty of the true position of the initial measuring point; $\delta v_{x0} = x_t(t_0, T_0) - v_x$ is the error resulting from uncertainty as to the true magnitude of the scale of transformation at the initial point; $R(t-t_0)$ is the error caused by variability in the scale of the transformation along the line of scan (because of nonlinearity); and $\Delta x_f(t - t_0, T - T_0)$ is the error resulting from geometric distortions. Since (see, e. g., [1])

$$R(t - t_0) \leq \frac{1}{2} \sup_t \left| x''_{tt}(t, T_0) \right| (t - t_0)^2 = \frac{M_2}{2}(t - t_0)^2,$$

$$\delta x \leq \delta x_0 + \delta v_x (t - t_0) + \frac{M_2}{2}(t - t_0)^2 + \Delta x_f.$$

Here

$$M_2 = \sup_t \left| x''_{tt}(t, T_0) \right|.$$

We choose the initial measuring point in the center, that is $t_0 = \frac{t_1 + t_2}{2}$. Thus the error in the region of the center will be minimal. Designating by X the dimension fo the field of view along the x-axis, that is, $X = v_x(t_2 - t_1)$, from (4) we obtain an estimation of the relative error

$$\frac{\delta_m x}{X} \leq \frac{\delta_m x_0}{X} + \frac{1}{2}\frac{\delta_m v_x}{v_x} + \frac{1}{8} M_2 \frac{t_2 - t_1}{v_x} + \frac{\Delta_m x_f}{X}, \qquad (5)$$

where $\delta_m x_0$, $\delta_m v_x$, $\Delta_m x_f$ are the corresponding maximum errors.

In order to calculate the value of M_2 it is necessary to know the specific form of the function $x(t,T)$. M_2 may be estimated if the nature of the function $x(t,T)$ is known, along with the coefficient of nonlinearity of transformation (1)

$$k_n = 2\frac{x'_{max} - x'_{min}}{x'_{max} + x'_{min}} \approx \frac{x'_{max} - x'_{min}}{n},$$

where x'_{max} and x'_{min} are the maximum and minimum scales of transformation in the scan line.

We assume that $x(t,T)$ may be approximated as a function of t by a polynomial of degree no higher than 3. As shown by experimental investigations, this is valid in instruments with high linearity in the variation of deflection currents. Then $x''_{tt}(t,T)$ is a linear function of t (see figure) and the coefficient of nonlinearity may be expressed in $x''(t,T)$ as

$$k_n = \frac{1}{v_x} \int_{t_{min}}^{t_{max}} x''_{tt}(t, T)\, dt, \qquad (6)$$

where t_{min} and t_{max} are the points at which x'_{min} and x'_{max} occur, respectively.

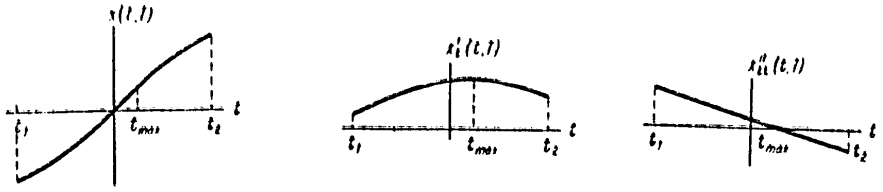

Graphs of the function x(t,T) and two derivatives with fixed T in the case of third-order nonlinearities.

Taking into account the fact that x"(t,T) is a linear function in t, we may write

$$\left|\int_{t_{min}}^{t_{max}} x''_{tt}(t, T)\, dt\right| \geqslant M_2 \frac{|t_{max} - t_{min}|}{2}, \tag{7}$$

so that strict equality holds in the case when $x''_{tt}(t,T)$ passes through zero within the interval (t_1,t_2).

From (6) and (7) for M_2 we obtain

$$M_2 \leqslant \frac{2k_{II} v_x}{|t_{max} - t_{min}|} \leqslant \frac{4k_{II} v_x}{t_2 - t_1}. \tag{8}$$

Taking this into account, the general expression for calculating the relative maximum error (5) may be written in the form

$$\frac{\delta_m x}{X} \leqslant \frac{\delta_m x_0}{X} + \frac{1}{2}\frac{\delta_m v_x}{v_x} + \frac{1}{2}k_{II} + \frac{\Delta_m x_r}{X}.$$

We note again that this expression was obtained with the assumption that nonlinear distortions were of order no greater than three. If we proceed from the assumption that x(t,T) is approximated by a second-order polynomial, then it may be shown that the $k_{II}/2$ term is replaced by $k_{II}/8$.

As an example we will examine measurement without calibration for typical values of parameters

$$\frac{\delta_m x_0}{X} = 0{,}05, \quad \frac{\delta_m v_x}{V_x} = 0{,}05, \qquad k_{II} = 0{,}05, \quad \frac{\Delta_m x_r}{X} = 0{,}04.$$

The maximum error is 14% of the size of the field and is reached at the edge of the field.

Measurement with a single reference point
This method is implemented in the following manner. Projected onto the photocathode of the detector, in addition to the image of the target, is a light point (the reference point) whose coordinates $x^{(o)}$ and $y^{(o)}$ are known precisely; coordinates t and T are measured with respect to this point and are taken as the initial t_o and T_o. Since $x_o=x(t_o,T_o)$ and $y_o=y(t_o,T_o)$ are known precisely, $\delta_m x_o = \delta_m y = 0$. Then from (5) we obtain

$$\frac{\delta_m x}{X} < \frac{1}{2}\frac{\delta_m v_x}{v_x} + \frac{1}{8}M_2\frac{t_2-t_1}{v_x} + \frac{\delta_m x_1}{X}.$$

If the nonlinearity of the transformation is of order no higher than three, then M_2 is estimated from formula (8). with the same data as in the previous example we obtain $\frac{\delta_m x}{X} < 9\%$, and the maximum error occurs at the edge of the field as before.

The use of a reference point in the center of the field of view makes it possible to achieve high accuracy in the central zone, where it is possible to ignore geometric distortions and nonlinearity. In a small central zone of size a we have

$$\frac{\delta_m x}{X} < \frac{1}{2}\frac{\delta_m v_x}{v_x}\frac{a}{X}.$$

With the same value of $\frac{\delta_m v_x}{v_x}$ as in the previous example, for a 10% central zone $\frac{\delta_m x}{X} < 0{,}25\%$, that is, the error resulting from raster instability may in practice be ignored. These results were confirmed experimentally under strict operational conditions.

Measurement with a coordinate grid without interpolation
This method is known in the literature as the method of measurement with descrete image partition [2]. For measuring x-coordinates the method entails projecting onto the photocathode of the transmitting tube a coordinate grid consisting of n+1 straight lines dividing the entire scan line into n equal intervals. A rough determination of the x-coordinate is made by counting the number of grid lines from the beginning of the coordinates to the target, and a precise determination is made by measuring the difference in raster coordinates between the target t and the last counted line $t^{(k)}$.

In exact measurement, the coordinate of lines $t^{(k)}$ is taken as the initial measuring point along the scan line within the interval $(t^{(k)},t^{(k+1)})$. The coordinate of $x^{(k)}$, corresponding to $t^{(k)}$, is known precisely, so $\delta_m x_o=0$. From (4) for points

in the interval $(t^{(k)}, t^{(k+1)})$ we have

$$\Delta x \approx \delta v_x^{(k)}(t - t^{(k)}) + \frac{1}{2} M_1 (t - t^{(k)})^2 + \Delta x_r^{(k)}(t - t^{(k)}, T - T_0), \quad (9)$$

where

$$\delta v_x^{(k)} = x_t'(t^{(k)}, T) - v_x;$$

$\Delta x_r^{(k)}(\cdot,\cdot)$ is the error resulting from geometric distortions in the interval $(t^{(k)}, t^{(k+1)})$.

For third-order nonlinearities the maximum relative error in speed is

$$\frac{\delta_m v_x^{(k)}}{v_x} = \frac{\delta_m v_x}{v_x} + k_{11}.$$

If the $t^{(k)}$-coordinate of the coordinate line is measured for T equal to the value of the T-coordinate of the target (that is, calibration is performed in the scan line in which the target is located), then in (9) it must be considered that $T-T_0=0$ and $\Delta x_r^{(k)}(t - t^{(k)}, T - T_0) = 0$.

Then, taking into account that

$$\max (t - t^{(k)}) = \frac{t_2 - t_1}{n}(1 + k_{11}),$$

from (9) in the case of third-order nonlinearity we obtain

$$\frac{\delta_m x}{\lambda} < \left(\frac{\delta_m v_x}{v_x} + k_{11}\right)\frac{1 + k_{11}}{n} + 2\left(\frac{1 + k_{11}}{n}\right)^2.$$

With the same parameters as previously and n=15 we have $\frac{\delta_m x}{\lambda} < 0{,}75\%$ for the entire field of view. In experimental investigations with n=15 and the number of raster partition elements 128x128, a total error resulting from raster distortions and from the discrete nature of the partition of less than 0.8% of the size of the field of view was obtained.

Measurement with interpolation

The problem of determining the target coordinates (x,y) from the known coordinates (t,T) may be approached differently. We will assume that the form of function (1) is unknown (as in fact it is). If values of functions (1) are known at several points $(t^{(i)}, T^{(i)})$, then by interpolation their values may be determined at any other point (t,T) not too far removed from points $(t^{(i)}, T^{(i)})$. The solution of this problem in the general form for functions of two variables encounters certain difficulties both in principle and in calculation. More expedient is interpolation according to each of the variables separately.

We will examine $x(t,T)$ for a certain fixed $T=\tilde{T}$. Then $x(t,\tilde{T})$ for $t \in [t_1,t_2]$ is a function of the single variable t. According to values $x^{(0)},x^{(1)},\ldots,x^{(n)}$, which $x(t,\tilde{T})$ assumes at points $t^{(0)},t^{(1)},\ldots,t^{(n)}$, it is necessary to determine the value of $x(t,\tilde{T})$ for any point $t \in [t_1,t_2]$. Such a problem may be solved, for example, with a Lagrangian polynomial of degree $nL_n(t)$ [3]. The interpolation error depends on the choice of interpolation points $t^{(0)},t^{(1)},\ldots,t^{(n)}$. If as interpolation points we choose roots of the Chebyshev polynomial of degree n+1 on the segment $[t_1,t_2]$, then the error will be minimal.

In measuring we may freely choose only the coordinates $x^{(i)}$ of the calibration marks. The $t^{(i)}$-coordinates are obtained through measurement. Therefore, in general, it is not possible to arrange for the interpolation points to coincide with roots of the Chebyshev polynomial. However, as a result of the approximately linear dependence of $x(t,\tilde{T})$, the interpolation points will coincide approximately with the roots of the Chebyshev polynomial on the segment $[t_1,t_2]$ if as the $x^{(i)}$ we choose roots of the Chebyshev polynomial of degree n+1 on the segment $[x_1,x_2]$.

As an example we will examine the simplest case n+1=2. Then

$$L_1(t)=\frac{x^{(1)}-x^{(0)}}{t^{(1)}-t^{(0)}}t+\frac{x^{(1)}t^{(1)}-x^{(0)}t^{(0)}}{t^{(1)}-t^{(0)}},$$

$$|x(t,\tilde{T})-L_1(t)|\leq\frac{1}{8}M_2(t_2-t_1)^2.$$

The roots of the Chebyshev polynomial are

$$x_1^{(0)}=\frac{\sqrt{2}}{4}(x_2-x_1)+\frac{x_2+x_1}{2};\qquad x_4^{(1)}=-\frac{\sqrt{2}}{4}(x_2-x_1)+\frac{x_2+x_1}{2}.$$

The error in this case may be estimated as follows:

$$|x(t,\tilde{T})-L_1(t)|\leq\frac{1}{16}M_2(t_2-t_1)^2.$$

For the same parameters as in the preceding examples, with a third-order nonlinearity we will have the following error values:

a) if x_1 and x_2 are taken as calibration points, then

$$\frac{|x(t,\tilde{T})-L_1(t)|}{X}\leq\frac{k_n}{2}=2,5\%;$$

b) if $x_4^{(0)}$ and $x_4^{(0)}$ are taken as calibration points, then

$$\frac{|x(t,\tilde{T})-L_1(t)|}{X}\leq\frac{k_n}{4}=1,25\%.$$

If more than two calibration marks are chosen and polynomials of higher degrees are used, then the interpolation error may be reduced. To calculate it, the maximum value of the derivative of the function $x(t,\tilde{T})$ of order n+1 must be estimated, and this is difficult in practice since the forms of the functions in (1) are not known to high precision.

When there are more than two calibration marks, it is possible to use linear interpolation in each of the intervals between successive interpolation points. If there are n+1 calibration points (n intervals), then the error may be estimated by the following expression:

$$|x(t, \tilde{T}) - L_1(t)| \leq \frac{1}{8} M_2 \left(\frac{t_2 - t_1}{n}\right)^2.$$

With n=15 for the same parameters as in the previous examples, in the case of nonlinearities of order not greater than three, the error will not exceed 0.01% of the size of the field of view.

Thus, using this or another calibration method, the error of an electrooptical instrument resulting from instabilities, deflection nonlinearities, and geometric distortions may be reduced to a negligibly small value. At the same time, in view of the ever expanding use of computer equipment to process measurement results, the implementation of complex interpolation algorithms providing extremely high precision is entirely practicable.

References

1. Korn G., Korn T., "Spravochnik po matematike dlya nauchnykh rabotnikov," [Handbook of mathematics for scientific workers], Moscow, NAUKA, Chief editorial board for literature in physics and mathematics, 1968.
2. Polonik V. S., "Televizionnyye avtomaticheskiye ustroystva," [Automatic television devices], Moscow, SVYAZ', 1974.
3. Berezin I. S., Zhidkov N. P., "Metody vychisleniy," [Calculational methods], Moscow, NAUKA, 1966.

Received by editors 25 August 1977.

9187
CSO: 8144/468

AN ILLUMINATING DEVICE FOR TESTING COORDINATE-SENSING PHOTODETECTORS

Leningrad OPTIKO-MEKHANICHESKAYA PROMYSHLENNOST' in Russian
No 8, 1978 pp 42-44

[Article by Ye. N. Vysotskiy, I. V. Reznikov, and A. N. Tikhomirov]

[Text] The optical design is described for an illuminating device having continuously regulable illumination and a field nonuniformity of 1.5%. Blurring at the edge of the image projected onto the photodetector is calculated.

High-quality light sources are the basic means for testing the parameters of coordinate-sensing photodetectors (cspd): dissectors, vidicons, scanistors, solid-state charge-coupled detectors, and so on. Features of the cspd's determine the quality criteria for light sources. For testing coordinate sensitivity over a field it is necessary to have sources with illumination nonuniformity not exceeding 2-3%. In determining the limit of output signal nonlinearity with respect to illumination and threshold sensitivity, sources are required having continuous regulation of illumination with unvarying color temperature. Illuminators produced by industry and described in the literature do not entirely satisfy these requirements. The four-channel illumination system of the EM-536 projector with the "Mikronar-600" objective lens has an illumination nonuniformity of approximately 5%, and in addition cannot be regulated in illumination and is complex to construct, align, and use. The raster illumination system described in [1] allows an illumination nonuniformity of greater than 5% at high illumination, and it also has some of the same characteristic shortcomings as the EM-536.

The design for testing cspd's using a distant light source and a mask placed directly on the cspd is both theoretically sound and practically proven. With this testing design the basic requirements are high illumination uniformity over the field and a minimal gap between the cspd and the mask.

Presented in fig. 1 is an illuminator using this design for testing cspd's. The SG-2 incandescent lamp, light source A, has a color temperature T=2854K [2]. The light-absorbing screen, 2, reduces bright spots on the back wall of the lamp casing, 3, and the bulb. Diaphragms, 4, forming the light channel, act as a blind for protection from bright spots occurring on the internal surfaces of the walls of the telescope tube, 5.

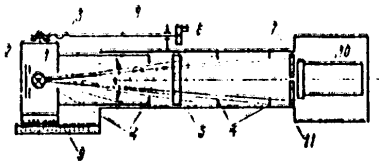

Fig. 1. Optical design of illuminator: 1 -- light source A (SG-2 incandescent lamp), 2 -- light absorbing screen, 3 -- lamp casing of illuminator, 4 -- light-restricting diaphragms, 5 -- telescope tube, 6 -- neutral light filters, 7 -- test mask, 8 -- tube displacement device, 9 -- readout device, 10 -- cspd tested, 11 -- light-tight chamber.

The positions of the diaphragms are chosen so that they eliminate first- and second-order bright spots [3,4], and in combination with the matte black coating of the inner surface with KhS-1107GM enamel they essentially prevent any light from the sides of the tube from reaching the cspd, 10. The diameters are chosen so that they continually narrow the illumination angle in order to prevent light diffracted from the edges of the diaphragms from striking the cspd. Neutral light filters, 6, allow the illumination of the cspd under test to be varied in steps. The mask, 7, forms the required test pattern on the cspd, depending on the test mode. The pattern on the mask (the test matrix) is produced by photolithography on a bimetal [5]. The metal mask, as distinct from a glass or film mask, makes it possible to create an image with 100% contrast, very important for testing dissectors and photomultipliers operating in the single-electron mode.

The use of a design with a distant light source and a system of light-restricting diaphragms has made it possible to achieve an illumination nonuniformity not greater than 1.5% over a field with a diameter of 35 mm.

Continuous variation of the illumination is achieved by moving the light source away from the cspd using a device for displacing the telescope tube, 8. In combination with

step-wise regulation by the light filters, the illumination is varied from 10 to 0.001 lx in the visible wavelength range. With continuous regulation the illumination varies in proportion to the square of the distance, so that within the limits of variation of the size of the telescope tube (400-500 mm) the illumination varies by a factor of 1.7 over all intermediate values, with the minimum variation determined by the scale value of the readout device, 9, -- 0.6%.

The degree of blurring of the edge of the image is determined by the distance l from the mask to the sensitive layer of the cspd (fig. 2). Taking into account the small viewing angle of the lamp filament, 1, in the mask opening, 2, it is possible to approximate with sufficient precision the degree of blurring of the edge of the image projected onto the cspd, 3, using the formula (not taking into account diffraction effects)

$$X = \frac{lb}{L},$$

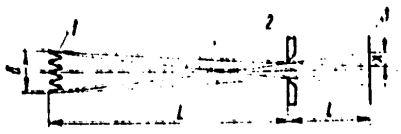

Fig. 2. For calculating the blurring of the edge of the projected image: 1 -- lamp filament, 2 -- mask with opening, 3 -- cspd tested.

where X is the degree of blurring of the edge of the projected image; l is the distance from the mask to the sensitive layer of the cspd; b is the size of the filament of the light source; and L is the distance from the filament of the light source to the mask.

With L_{min}=400 mm, b=1 mm, and l=4 mm we obtain X=10 μm, which in many cases is considerably less than the resolving power of the cspd.

The distance from the mask to the sensitive layer of the cspd is determined by the thickness of the glass envelope, which ranges from 2 to 4 mm.

For solid-state charge-coupled detectors the degree of blurring may be considerably less (less than 1 μm) because of the reduction in the magnitude of l.

The degree of blurring of the edge of the projected image is taken into account in testing the resolving power of the cspd for given parameters of the test matrix on the mask.

The illuminator described is relatively simple to construct and completely satisfies cspd testing requirements for nonuniformity and continuous regulability of illumination, contrast, and degree of blurring of the edge of the projected image.

References

1. Bolotnikov V. A. et al., ELEKTRON. PROMYSH., 1975 no. 6, p. 29-34.
2. Karalis V. N., Korneyeva E. A., "Apparatura dlya fluorestsentnogo analiza," [Apparatus for fluorescent analysis], Moscow, Committee for standards, measures, and measuring instruments of the USSR Council of Ministers, 1970, p. 27.
3. Sakin I. L., "Inzhenernaya optika," [Engineering optics], Leningrad, MASHINOSTROYENIYE, 1976, pp. 151-154.
4. Kruger M. Ya. et al., "Spravochnik konstruktora optiko-mekhanicheskikh priborov," [Handbood for the designer of optical engineering instruments], Leningrad, MASHINOSTROYENIYE, 1968, pp. 385-390.
5. Medvedeva I. Ye. et al., OPT.-MEKH. PROMYSH., 1976, no. 2, p. 73.

Received by editors 20 July 1977.

9187
CSO: 8144/468

METHOD FOR DETERMINING THE NONLINEARITY OF PHOTODETECTORS

Leningrad OPTIKO-MEKHANICHESKAYA PROMYSHLENNOST' in Russian
No 8, 1978 pp 59-61

[Article by L. N. Aksyutov and G. K. Kholopov]

[Text] A method is described for numerically determining the nonlinearity of photoelectric radiation detectors, based on the measurement of their relative differential sensitivity as a function of the magnitude of the output signal.

In order to make precise photometric studies, the ratio between the magnitude of the output signal of the detector system and the measured magnitude must be known over the entire range of the detector. This requirement is satisfied if the detector system is linear. The linearity of a detector system in which a photodetector acts as the sensing element is judged by its energy response characteristic. However, it is known that nonlinear distortions in photodetector electrical circuits depend not only on the magnitude of the light flux incident on the detector, but also on parameters of the electrical circuit [1]. Thus linearity of the energy response characteristic of the photodetector is not sufficient to guarantee linearity of the detector system as a whole. Consequently, for testing the linearity of a detector system or estimating its nonlinearity, special measurements must be made using the system.

The essence of traditional methods for determining the nonlinearity of radiation detectors [2] is the creation of a known level of illumination at the detector or the variation of the illumination according to a known law, presupposing graduation or calibration of the measuring equipment.

The object of this article is to demonstrate the capabilities of a method for numerical estimation of the nonlinearity of photodetectors, based on the measurement of characteristics

of their relative differential sensitivity. The method does not assume knowledge of the magnitude of detector illumination, nor of the law governing its variation.

The nonlinearity of a photodetector is determined by the relative variation of its sensitivity at differing illumination levels and is expressed by the value of the coefficient of nonlinearity [3]

$$K=(S/S_0)-1 \tag{1}$$

where S is the sensitivity of the detector to a certain radiation flux producing an output signal N and a corresponding illumination E; S_0 is the sensitivity of the detector to a certain arbitrarily chosen flux, corresponding to illumination E_0, which produces an output signal N_0. In practice E_0 corresponds to minimal light fluxes incident on the photodetector, and E to any value of the flux in the dynamic range of measured values. Thus it is assumed that $E > E_0$.

In accordance with expression (1) a linear detector, for which $S=S_0$, is characterized by the value K=0. When K=const$\neq$0, the detector is also linear, but its sensitivity is different from S_0. The criterion of detector nonlinearity is K$\neq$const, with $K > 0$ corresponding to the case in which detector sensitivity increases with increasing illumination, that is, "superlinear" sensitivity, and with $K < 0$ corresponding to the case in which sensitivity decreases with increasing illumination, that is, "sublinear" sensitivity.

Since for detector sensitivity S we are taking the ratio of its output signal N produced by illumination E to the magnitude of this illumination, expression (1) may be rewritten in the form

$$K=(NE_0/N_0E)-1 \tag{2}$$

In accordance with the energy response characteristic of the detector, the value of the illumination is determined by the expression

$$E=\int_0^N (\partial N/\partial E)^{-1}\,dN=E_0+\int_{N_0}^N (\partial N/\partial E)^{-1}\,dN. \tag{3}$$

Substituting (3) in (2) we obtain

$$K=\left\{N/\left[N_0+\int_{N_0}^N dN/\beta(N)\right]\right\}-1, \tag{4}$$

where $\partial N/\partial E$ is the differential sensitivity of the detector [1]; $\beta(N)=(\partial N/\partial E)/(N_0/E_0)$ is the relative differential sensitivity characteristic of the detector.

Expression (4) indicates the possibility of determining the nonlinearity of photodetectors according to the known value of the output signal when, rather than the value of the illumination, the differential sensitivity of the detector is measured as a function of the magnitude of the output signal N. In this case the value of the differential sensitivity with background illumination $E \approx 0$ corresponds to output signal N_0 produced by a modulated flux (the signal flux [1]), created at the detector by an additional illumination E_0 above background. If the background illumination E (the background flux [1]) is increased, then the changed value of the differential sensitivity at a constant value of the signal flux (E_0=const) corresponds to the changed value of the output signal N_0^*.

Taking measurements of the function $N_0^*=f(E)$ similar to measurements of the background characteristic [4], and simultaneously measuring the value of output signals N with identical modulation of the background flux produced by the total illumination $E+E_0$, it is possible to construct the relative differential sensitivity characteristic of the detector $\beta(N)=N_0^*/N_0$. This function, according to formula (4), determines the value of the coefficient of nonlinearity K for a given magnitude of the output signal from the detector.

From formulae (2) and (4) it follows that the numerical value of the nonlinearity, expressed by the coefficient K, for a given value of the output signal N will differ depending on the value taken for N_0. In practice the value of N_0 is determined by the minimum signal-to-noise ratio, established for the specific case, and the maximum value of N is determined by the values of illumination at which the detector sensitivity begins to saturate. Knowing the nonlinear characteristic of the photodetector and the value of illumination corresponding to a particular value of N, it is possible to construct its energy response characteristic as needed.

To illustrate the foregoing we present results of the determination of detector nonlinearity obtained by the method of measuring the relative differential sensitivity. The measurements were performed on a device [5], one of the versions of which is shown in fig. 1. The design of the source, 1, and its placement relative to the detector studied provides for variation in the background illumination proportional

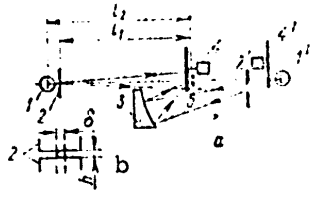

Fig. 1. Diagram of the measuring device: a) 1 -- source of background flux; 1' -- source of signal flux; 2, 2' -- slit/diaphragm; 3 -- spherical mirror; 4, 4' -- modulators; 5 -- photodetector tested; b) relative positions of incandescent elements of source: 1 -- tungsten ribbon of width and slit, 2, of width h.

to the width of the slit, 2, making it possible to measure the energy response characteristics of detectors on this device.

Fig. 2 shows differential characteristics of CdS photodetectors measured for two values of N_0 at each modulation frequency. The displacement of curves 1 and 3 along the N-axis relative to curves 2 and 4 is caused by the increased sensitivity of the photodetector at a modulation frequency of 450 Hz, though the maximum values of β correspond to the same value of illumination in each case. The form of the $\beta(N)$ curves indicates that the sensitivity of the photodetector is superlinear over the entire range of measured signals and that there are no linear segments in its energy response characteristic. Clearly the determination of the nonlinearity of photodetectors with superlinear sensitivity used as radiation measuring instruments is meaningful only at values of energy illumination at which sensitivity saturation has not yet occurred. This value (see fig. 2) corresponds to the maximum output signals for which $\beta(N) \approx 1$.

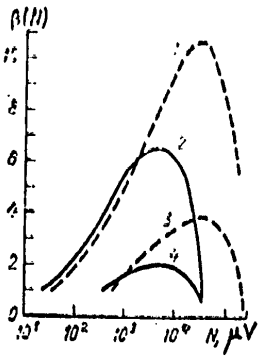

Fig. 2. Relative differential sensitivity characteristic of CdS photoresistor: N_0=36[1], 21[2], 500[3], 360[4] μV; 1,3 -- 65 Hz; 2, 4 -- 450 Hz.

Nonlinearity characteristics for a CdS photodetector were calculated from $\beta(N)$ characteristics using formula (4) and are presented in fig. 3.

The reproducibility of results of nonlinearity determinations by this method was established by us earlier [3] in the study of a photomultiplier, for which the deviation from linearity was relatively small. Comparison of the energy response characteristics of the CdS photodetector calculated from results of the nonlinearity determination with those measured directly (see fig. 4) demonstrates the reproducibility of the results for large nonlinearities as well.

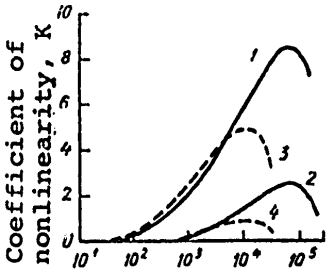

Fig. 3. Nonlinearity characteristic for CdS photoresistor: 1, 2 -- 65 Hz; 3, 4 -- 450 Hz.

We have used this method and the measuring device whose design is shown in fig. 1 to determine the nonlinearity of radiometers. As an example we may cite the results of determining the nonlinearity of two specific radiometers with PbS and InSb photoresistors as the sensing elements. The relative differential sensitivity characteristic of these radiometers is of the sublinear sensitivity type and may be espressed by a function of the form

$$\beta(N) = 1 - \alpha N, \qquad (5)$$

where for the PbS radiometer: $\alpha = 0.19\ V^{-1}$, $N_o = 10N_n = 7mV \leq N \leq 3V$; for the InSb radiometer: $\alpha = 0.021\ mV^{-1}$, $N_o = 10N_n = 250\mu V \leq N \leq 25$ mV; N is the output signal value; and N_n is the noise value at the output of the radiometer.

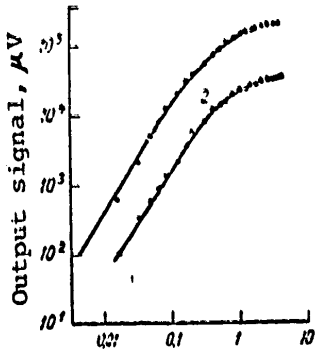

Fig. 4. Energy response characteristic of CdS photoresistor: 1 -- 65 Hz; 2 -- 450 Hz; solid lines are calculated curves; circles are experimental data.

In accordance with equations (4) and (5), the value of the coefficient of nonlinearity of the radiometers is expressed by the formula

$$K = -\frac{\alpha N}{\ln(1-\alpha N)} - 1.$$

As demonstrated in the practical determination of the nonlinearity of photodetectors by the method of measuring their relative differential sensitivity, this method of testing nonlinearity has the following advantages over traditional methods:

1. No calibration or graduation of the measuring equipment is required.

2. Use of the method is independent of the polarization of the radiation and of the polarization properties of the apparatus tested.

3. Results of determining the nonlinearity are reproducible regardless of its magnitude.

4. The method requires little labor and only simple equipment.

5. Nonlinearity may be tested with various spectral compositions of the signal and background fluxes.

References

1. Korndorf S. F. et al., "Raschet fotoelektricheskikh tsepey," [Design of photoelectric circuits], Moscow, ENERGIYA, 1967.
2. Aksyutov L. N., Kholopov G. K., OPT.-MEKH. PROMYSH., 1973, no. 10, p. 42.
3. Aksyutov L. N., Kholopov G. K., OPT.-MEKH. PROMYSH., 1971, no. 10, p. 65.
4. Astaf'yev A. I., Kholopov G. K., OPT.-MEKH. PROMYSH., 1969, no. 10, p. 1.
5. Aksyutov L. N., Kholopov G. K., Melent'yeva L. F., Inventor's certificate no. 458715, BYUL. IZOBR., 1975, no. 4.

Received by editors 3 October 1977.

9187
CSO: 8144/468

UDC 535.317.7

AUTOMATING THE PROCESSING OF INTERFEROGRAMS IN THE TESTING OF OPTICAL SYSTEMS

Leningrad OPTIKO-MEKHANICHESKAYA PROMYSHLENNOST' in Russian No 9, 1978 pp 7-10

[Article by Candidate of Sciences V. A. Zverev, I. P. Agurok, Candidate of Sciences S. A. Rodionov and Candidate of Sciences M. N. Sokol'skiy]

[Text] The mathematical apparatus and the programming system for computer programming of interferograms and a method of eliminating errors produced by the interferometer are presented. These will make it possible to determine the topography of wave front deformation and the main quality characteristics of the optical image. The results of processing of interferograms obtained during testing of a hyperbolic mirror with a diameter of 1,100 mm are presented.

The interference method is traditional in the testing of optical systems and surfaces. Visual evaluation of interferograms makes it possible to determine the extent and position of local wavefront deformations, as well as astigmatisms. However, computer processing of the results is necessary in order to utilize most fully the possibilities of the method and to obtain the necessary information about a mirror surface or the wave aberration of an optical system, or to determine the quality characteristics of an optical image. This article describes the automation of interferogram processing during testing with an unequal-path interferometer.

Obtaining the Interferogram

The system for testing with an unequal-path interferometer is well known (Fig. 1-a). However, in order to reconstruct with good quality a wavefront deformation it is necessary to allow for errors produced by the system itself, some of which can be eliminated by subsequent computer processing, and others of which can be minimized by following the recommendations presented below.

/Errors which cannot be eliminated by subsequent computer processing./ These include a discrepancy between the recording surface 7 and the surface next to the output pupil of the system being tested, since in this case deformation of

the wavefront on surface 7 will result in an observed shift of the wave phase because the wavefront is propagating equidistantly while diffraction phenomena are affecting it strongly. In the testing of optical systems we are interested in the deformation of the wavefront in the plane of the exit pupil, just as in testing of the surfaces of manufactured parts, since the main aim is to determine quality characteristics of the optical image on the basis of the scalar theory of diffraction, in which it is desirable to use the wavefront in planes where the Kirchhoff conditions are adhered to, i.e. in the system pupils [2, 4]. A second error results fron the difference between the shape of the recording surface and the nearest comparison sphere of the wavefront, which produces distortion. This occurs when the forward focus of the objective 6 does not coincide with the autocollimation point A of the system (Fig. 1-b).

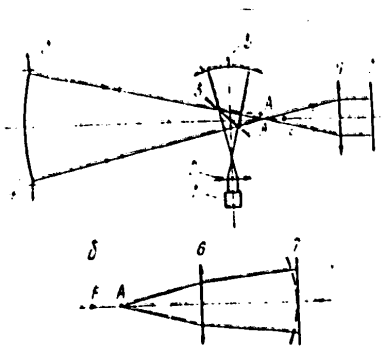

Fig. 1. The Optical System

Key: 1. Laser
2. Focusing objective
3. Beam splitter
4. Surface under test
5. Standard sphere
6. Objective
7. Film plane

In experimental practice, of course, it is impossible to eliminate these errors completely. But minimization of FA (Fig. 1-b) to within 1-3 mm and focusing of the objective 6 on the pupil will guarantee that their effect will be insignificant.

/Errors which can be eliminated by subsequent processing./ We will consider the causes of these errors. Methods of eliminating them are described in the next section. They include longitudinal and transverse defocusing resulting from the shifting of points A and A' (Fig. 1-a), introduced to produce the required type of interference pattern; inclination of the photographic objective with respect to the axis of the beam leaving the system, leading to distension in the interferogram equivalent to additional astigmatism; and inaccuracies in the manufacture of the standard mirror and additional spherical aberration arising with apertures greater than 0.30.

Obtaining Digital Information

In order to process by computer the information in the interferogram, it must be converted to discrete digital form. For this purpose the interferogram is measured. The measurement procedure depends on the mathematical apparatus for reconstruction of the wave aberration function. An interferogram on film is measured using a UIM-21 (23). The distances from the axis of rotation of the measuring table to the points of intersection of rings by radii at angles selected so as to encompass all the characteristics of the interferogram, or the X,Y coordinates of the rings (or fringes), are measured. In addition the X and Y coordinates of 10-20 points on the edge of the pupil are measured. The

main source of noise in measuring the coordinates of the rings is the indeterminacy of the position of the object of interest, the photometric maximum (minimum) of a fringe, when observing with a visual instrument. Its relative size is about ± 0.05--0.08 of the visible breadth of the fringe.

Mathematical Apparatus

/Elimination of the error resulting from inclination of the axis of the photographic objective relative to the axis of the beam leaving the system being tested./ In order to eliminate this error we must determine the ellipticity of the pupil border in the interferogram and correct the measurement results to a circular pupil. The coordinates of the center of the pupil are determined in advance as the arithmetical results of measurement of the X and Y coordinates of points on the pupil border. The coordinates of XO and YO thus derived are the starting point for a nonlinear least-squares analysis, involving minimization of

$$\sum_{i=1}^{N}\left[R_{cp}-R_i-\frac{\partial R_i}{\partial C_X}\Delta C_X-\frac{\partial R_i}{\partial C_Y}\Delta C_Y\right],$$

where

$$C_X \equiv XO;\ C_Y \equiv YO;\ R_i=\sqrt{(X_i-XO_j)^2+(Y_i-YO_j)^2};$$

$$R_{cp}=\frac{\sum R_{ij-1}}{N};$$

and j is the index of the iteration interval [1].

The pupil border is given in polar coordinates as follows:

$$\rho = r + a\cos 2(\psi - \alpha),$$

where ρ and ψ are the radius vector and the polar angle; and p, a and α are unknowns. To determine the unknown parameters we use the following series of relationships in discrete form:

$$\int_0^{2\pi}\rho\,d\psi = 2\pi r \int_0^{2\pi}(\rho - r)^2\,d\psi = a^2\pi \int_0^{2\pi} XY\,d\psi = ar = \sin 2\alpha .$$

The resultant r, a and α are the initial conditions for the nonlinear least-squares analysis with convergence criteria $\Delta r = 10^{-3}$, $\Delta a = 10^{-3}$, $\Delta\alpha = 5 \cdot 10^{-4}$ rad. These parameters must be determined beforehand, since the least-squares method may converge to a false extremum. [1]. Real values for a are about 0.05.

/Reconstructing the wave aberration for the system being tested./ The interferogram being studied reflects the wave aberration we are seeking with defocusing. The rings (fringes) of the interference pattern are the degrees of discretization of the wavefront by λ . The defocusing is an additional function and must be eliminated:

$$P(X,Y) = C0 + C1 \cdot X + S1 * Y + C20 \cdot (X^2 + Y^2). \quad (1)$$

The defocusing is eliminated by the least-squares method with the criterion

$$\sum_{i=1}^{N} [F(X_i; Y_i) - P(X_i; Y_i)] = \min,$$

where the summation is carried out for all measurements, giving the minimum mean square wave aberration, and accordingly the maximum Strehl number [2]. The fact that the total defocusing produced in the interferometer system and contined in the wave aberration of the system is eliminated means that analysis of the image quality will be carried out on the optimal plane of the apparatus and at the optimal point on it. In the operation of a spherical mirror, the spherical aberration which is linearly dependent on C20 (1) does not arise from the aplanatic point or an aspherical mirror with a corrector under the same conditions.

Here (with an aperture greater than 0.35) the defocusing is eliminated using a K determined in advance by calculation from the test system:

$$\sum_{i=1}^{N} [F(X_i; Y_i) - P(X_i; Y_i); - K \cdot C20 \cdot (X_i^2 + Y_i^2)] = \min. \quad (2)$$

In order to construct the wave aberration diagram of the system in question, which is required, for example, in industrial testing of mirrors, and also for image quality analysis, it is necessary to reconstruct a two-dimensional wave aberration function. This function is reconstructed by a least-squares approximation with analysis of the significance of the coefficients that have been derived, making it possible to eliminate measurement noise. Three variants of least-squares approximation have been developed.

The first method makes use of Zernike's polynomials, orthogonal on a circle. The system of normal least-squares equations is solved by the Gauss method. As indicated in [7], the number of operations required in solution of a system of linear equations by the Gauss method is close the the theoretical minimum. Operation of the program in the test mode indicates a good degree of dependence in the system of linear equations.

The second approximation method also uses the Zernike polynomials, but the system of normal equations is solved by the orthogonalization method [1, 8]. The selected basis (the Zernike polynomials) is orthogonalized on a random sampling function using the Gram-Schmidt method [8]. Neither of these programs requires prior elimination of defocusing, since the defocusing polynomials are present in the basis selected and the approach to elimination of defocusing described above is retained.

In the third variant, the system of normal equations is also solved by the method of orthogonalization, but the orthogonal basis is produced as described below. This method requires measurements along the radii. The defocusing is eliminated beforehand in accordance with (2). On each measured radius, we construct according to the Forsythe relationship [1, 3] the orthogonal basis $Q_{im}(\rho)$, where m is the number of radii and i is the degree of the polynomial, after which we construct an orthogonal basis in $\varphi - \psi_j(\varphi)$ on the sampling function

function for the radial angles. We treat the polynomials Q_{im_1} as a single polynomial ($m_1 = \text{const}$) by joining the coefficients of the Forsythe recurrence relations by splines. It is easily seen that the basis $\Psi_j(\varphi) * Q_j(\rho)$ is also orthogonal. This method is promising for large sampling functions. After finding the coefficients we analyze their significance by the test [1]

$$(\hat{z} - Q\hat{\theta})' (QD(0)Q')^{-1} (\hat{z} - Q\hat{\theta}) \leq F_{b,n-m},$$

where $\hat{\theta}$ is the vector of the coefficients obtained, D(0) is the covariation matrix for evaluation of the parameters and $Q_b * {}_m\hat{\theta}_m = z_b$ is the hypothesis.

In the second and third variants we analyze the hypothesis $\hat{\theta}_i = 0$, where $i = 1, 2, \ldots, m$ ($b = 1$, $Q = (0, 0, 1, \ldots, 0; z = 0)$, while in the first variant we analyze a more complex hypothesis in which $b = 2$, i.e. the coefficients are analyzed in pairs starting with θ_i and θ_{i+1}, and then additionally with the highest correlations. Next the error of the standard mirror which has been determined in advance by the three-mirror method is subtracted from the reconstructed wave aberration.

In cases of large local errors we use the second method of reconstruction of the wave aberration, and in cases of smooth wave aberrations we use the first; the existence of program systems with several methods for reconstructing the wave aberration makes for high quality and reliability of results.

Analysis of Image Quality of the System Under Test

Analysis of image quality entails determination of diffraction point spread functions, the energy concentration function and the two-dimensional optical transfer function. According to the scalar theory of diffraction [2, 4], the point spread function is determined by applying the fast discrete Fourier transform (FDFT) method to the pupil function. Introductions to the FDFT algorithm are given in [5] and [6]. A special version of the fast Fourier transform algorithm without bit inversion and with a shift in the coordinate origin, without an increase in the number of operations, which uses zeroes bordering the pupil function, has been developed. To determine the OPF [optical transfer function], an algorithm for transformation of the real function is used. The energy concentration function (FKE) is computed by integrating the point spread function (PSF [FRT]) over circular domains by the Simpson method. The energy concentration function, the point spread function diagram, the frequency-contrast and frequency-phase cross sections and the frequency-contrast curve on a logarithmic scale are output on a printer.

We illustrate the use of this mathematical apparatus and the computer programs to perform calculations on interferograms through the example of testing of the main hyperbolic mirror, 1,100 mm in diameter, of the AZT-24 telescope. The interferogram shown in Fig. 2 was obtained from the center of curvature of the mirror with a spherical aberration compensator applied to the mirror. Fig. 3 shows the wave aberration contours of the mirror after selection of the optimal comparison sphere. The printer also produced a cross section of the surface deviation from the ideal over 45°, the point spread function, the frequency frequency-contrast curve and a contour map of the point spread function and the frequency-contrast curve. Fig. 4 shows a graph of the frequency-contrast curve and the energy concentration curves. The broken lines are for the ideal system.

The calculations were made for $\lambda = 0.63$ microns and a central screening value of 0.5.

This automated method for interferometric testing has a high information value and is accurate and fast, rendering it applicable for industrial and certification testing of large-scale optics.

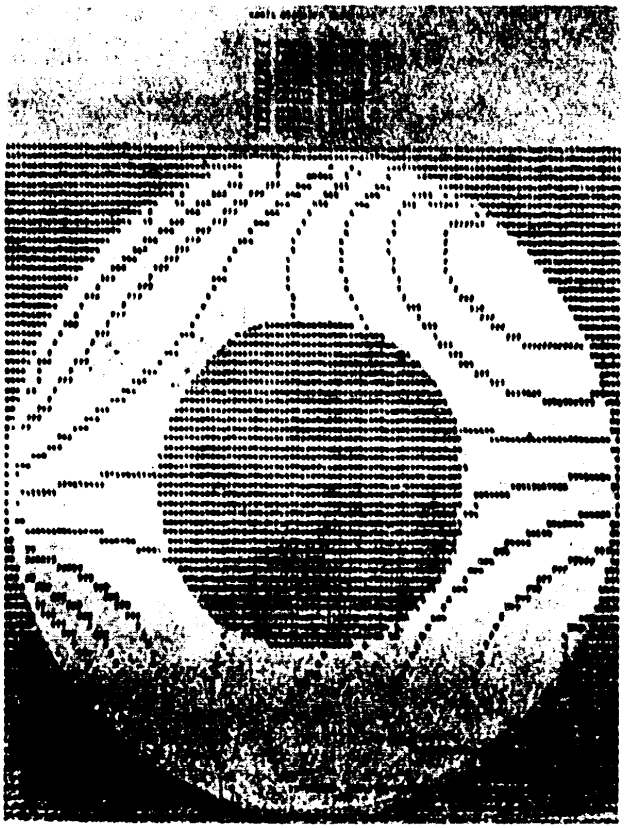

Fig. 3. Wave Aberration Contours of Mirror

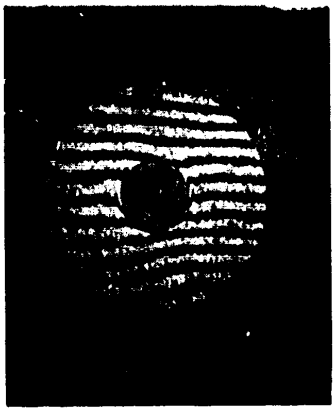

Fig. 2. The Interferogram

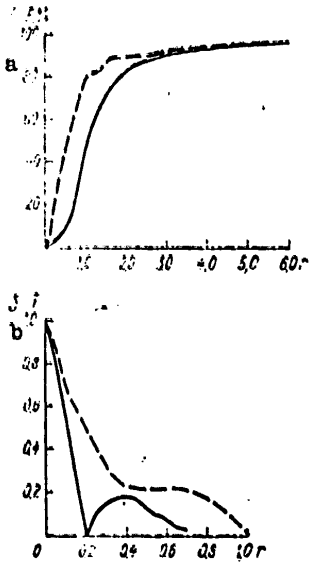

Fig. 4. a: Energy distribution in scattering spot.

Central screening 0.5 ($r = \lambda/a$ is the radius of the diffraction scattering spot; u is the rear aperture).

b: Frequency-contrast characteristic T.

BIBLIOGRAPHY

1. D. Hudson. Statistics for Physicists. Mir, 1970.

2. M. Born; and E. Wolf. Fundamentals of Optics. Nauka, 1970.

3. R. V. Hemming. Numerical Methods. Nauka, 1972.

4. G. Goodman. Introduction to Fourier Optics. Mir, 1970.

5. J. W. Cooley; and J. W. Tukey. "An Algorithm for the Machine Calculation of Complex Fourier Series," MATH. COMP., 19 (April, 1965).

7. Forsythe, Moler. Numerical Methods for Solving Systems of Linear Equations. Mir, 1969.

8. Bakhvalov. Chislennyye metody [Numerical methods]. Nauka, 1975.

Received 16 January 1978.

8480
CSO: 8144/0469

UDC 535.81:778.4

COMPUTER PROCESSING OF INTERFEROGRAMS AND DETERMINATION OF THE POINT SPREAD FUNCTION AND OPTICAL TRANSFER FUNCTION IN TESTING AND FINISHING OF OPTICAL SYSTEMS

Leningrad OPTIKO-MEKHANICHESKAYA PROMYSHLENNOST' in Russian No 9, 1978
pp 25-28

[Article by M. A. Gan, S. I. Ustinov, V. P. Kotov, P. A. Sergeyev and I. N. Tsvikevich]

[Text] A method for constructing a complete contour map of wavefront deformations and calculating optical transfer functions (OPF) from the results of interferogram processing is discussed. The method is based on approximation of wave aberrations by polynomials which are orthogonal over a discrete set of points and utilization of the fast Fourier transform. It is demonstrated that calculation of optical transfer functions for actual wave aberrations is in good agreement with results from recording of two-dimensional optical transfer functions by the holographic method.

The high requirements for image quality of modern optical systems for various purposes such as large-size astronomical and photographic systems [1], objectives for microelectronics, optical systems for coherent computer devices [2] and so on require not only design of practically aberration-free systems but also accurate testing, assembly and adjustment of optical products.

Accordingly it is a pressing problem to determine the level of acceptable residual aberration and to compensate manufacturing defects in optical parts on the basis of results of wavefront deformation testing. Since the acceptable level of aberration is determined by the diffraction structure of the image, it is necessary to calculate the point spread function (PSF [FRT])--the image of a star--and the optical transfer function (OTF [OPF]) for the real wave aberration of a system during its finishing and testing.

Quantitative analysis of the effect of manufacturing defects is apparently carried on by the leading foreign companies [13-15], which in combination with an automated retouching process enables them to significantly speed up the finishing of complex optical systems.

Real wave aberrations are usually not symmetrical, which makes the task of presentation of the calculation results required for decisions regarding correction of the optical system significantly harder. In addition to calculation of such generalized criteria as the standard deviation of the wavefront and the Strehl number [3], methods for the presentation of two-dimensional point spread functions and optical transfer functions using computer-controlled alphanumeric printers and graph plotters are necessary.

The remarkable properties of the Twyman interferometer [4] as a device for testing optical systems were noted as early as the 30's by many investigators [5, 6], but extensive application of this method was hindered by the lack of a source of light with a large coherent length. In addition, the processing of interferograms by graphic or graph-analytic methods required long periods of time.

The development during the last decade of effective methods for computing Fourier transforms and the use of computers has speeded up the processing and interpretation of interferograms. The use of the laser as a light source made it possible to develop a compact and rather universal unequal-path interferometer [7], which is apparently the most widespread and convenient method for testing wavefront deformation in both the assembly and the final testing of optical systems.

Holographic optical components (GOE) are used in image formation systems and in optical information processing devices. The interferometric method is suitable for testing these components, since the recording device is easy to change over for testing of the wavefront to be reconstructed by these components.

Illumination extrema appear on the interferogram as a line of constant phase difference between the reference wavefront and a wavefront which has passed through the optical system (if the tests are carried out with an autocollimated device it is necessary to allow for the Q factor for passage of the light through the optical system under test.

After the coordinates of the interference fringes have been measured and the corresponding numbers assigned, we obtain the values W_R for the discrepancy between the wavefront being studied and the reference wavefront over a system of points $\{(X, Y)_{ij};\ i=1, n;\ j=1, p_i\}$, where i is the number of the interference fringe. Accordingly the wavefront discrepancy W_R can be written as $W_R(x, y)_{ij} = \lambda i/Q$, where λ is the wavelength of the light used to make the interferogram. According to the superposition theorem [3],

$$W_R = W + W_{SR}, \qquad (1)$$

where W is the wave aberration relative to the nearest reference sphere and (for small aberrations)

$$W_{SR}(X, Y) = D(X^2 + Y^2) + L_X x + L_Y y + C. \qquad (2)$$

where D, L_X, L_Y and C are parameters characterizing the transition from the reference sphere for which the interferogram was obtained to the nearest sphere for the wavefront being studied.

In general the system of points $\{(X, Y)_{ij}\}$ is irregularly distributed over the surface of the interferogram and the selection of the reference sphere is not the best possible for assuring minimum deviation from the wavefront being tested; moreover, inclination or defocusing of the reference front makes it easy to number the fringes, so that additional processing of the fringe coordinates is necessary to obtain the distribution of the wave aberrations W. This processing comprises two stages: determining the optimal parameters of the reference sphere, and interpolation of the wave aberrations W for a nonuniform pattern $\{(X, Y)_{ij}\}$. The latter is necessary both for presentation of the wave aberrations in the form of contour maps and for the computation of the point spread function and the optical transfer function.

Both stages of the processing of the interferogram can be carried out by approximating the function W_R by a system of functions $a_{n,m}\psi_{n,m}$ ($\psi_m \equiv X^nY^m$), while the coefficients $a_{n,m}$ can be obtained by the classical least-squares method [1]. This requires the setting up of a system of normal equations. We carry out a sequential numeration of the points $(X, Y)_{ij} = (X, Y)_k$, $k = 1, N$, where $N = p_1 + \ldots + p_n$, and of the quantities $W_{Rij} = W_{Rk}$, as well as a sequential numbering of the coefficients $a_{n,m} = a_\ell$ and of the functions $\psi_{n,m} = \psi_\ell$, where $\ell = ((m+n)^2 + 3m + n)/2$. Then the system of normal equations takes the form

$$\sum_{l=0}^{L} a_l [\psi_l \psi_q] = [W_R \psi_q], \quad q = 0, \ldots, L,$$

where $L = M(M+3)/2$; M is the maximum degree of the two-dimensional polynomial ψ_ℓ; and [] are Gaussian brackets indicating summation over k from 1 to N.

The coefficients of the system of normal equations depend on M, and accordingly to increase the degree of the polynomial from M to M+1 it is necessary to set up and solve a new system of L equations for a new value of M; in order to avoid this difficulty we carry out an expansion of the function W_R to be approximated, in terms of functions φ_ℓ which are orthogonal over the discrete set of points $\{(X, Y)_k\}$ and normalized, i.e.

$$[\varphi_l \varphi_q] = \begin{cases} 1 & l = q \\ 0 & l \neq q. \end{cases}$$

The system of functions φ_ℓ can be obtained by orthogonalizing the system of independent function ψ_ℓ by the Gram-Schmidt method (functions which are linearly dependent over the system of points $\{(X, Y)_k\}$ must be excluded).

Suppose that $\ell - 1$ coefficients $\alpha_i^{(\ell-1)}$ of the expansion of W_R by the system of functions ψ_i have been calculated; then the non-normalized orthogonal function $\tilde{\varphi}_\ell$ corresponding to ψ_ℓ is determined by the following formula:

$$\tilde{\varphi}_l = \sum_{i=0}^{l-1} \mu_{l,i} \varphi_i + \psi_l, \qquad (3)$$

where

$$\mu_{l,i} = -[\psi_l \varphi_i].$$

In addition we calculate the non-normalized coefficients $\tilde{\gamma}_{l,i}$:

$$\left.\begin{aligned}\tilde{\gamma}_{l,l} &= 1, \quad \text{если} \quad l = l,\\ \tilde{\gamma}_{l,i} &= \sum_{j=i}^{l-1} (A_{l,j}\gamma_{j,i}, \quad \text{если} \quad 0 < i < l.\end{aligned}\right\} \qquad (4)$$

Next we normalize

$$\left.\begin{aligned}\varphi_l &= \tilde{\varphi}_l/(|\tilde{\varphi}_l\tilde{\varphi}_l|)^{1/2},\\ \gamma_{l,i} &= \tilde{\gamma}_{l,i}/(|\tilde{\varphi}_l\tilde{\varphi}_l|)^{1/2}.\end{aligned}\right\} \qquad (5)$$

Now it is simple to compute the coefficient β_l in the expansion of W_R corresponding to φ_l and the changes in the coefficients α_i $(0 \leq i \leq l)$

$$\beta_l = |W_R\varphi_l| \qquad (6)$$

and

$$\left.\begin{aligned}a_l^{(l)} &= \beta_l\gamma_{ll},\\ a_i^{(l)} &= a_i^{(l-1)} + \beta_l\gamma_{il} \quad (0 < i < l-1).\end{aligned}\right\} \qquad (7)$$

The condition for termination of the calculation is either attainment of the required accuracy (evaluated by standard deviation or the absolute value of the maximum deviation at each point) or attainment of the specified degree of the polynomial.

In addition, statistical analysis and evaluation of the significance of the difference from zero of the coefficients β_l is carried out according to the Fisher test [9]. The initial conditions are given for $l = 0$ by the following relationships:

$$\varphi_0 = \tilde{\varphi}_0 = 1.$$

Calculating the first coefficients $0 \leq l \leq 5$ makes it possible to determine the optimal (in terms of standard deviation) values of the parameters W_{SR}:

$$\left.\begin{aligned}C &= a_0 = a_{00};\\ L_x &= a_1 = a_{10};\ L_y = a_2 = a_{01};\\ D &= (a_3 + a_5)/2 = (a_{20} + a_{02})/2.\end{aligned}\right\}$$

In addition the effective value of the astigmatism A and its orientation are calculated:

$$\left.\begin{aligned}A &= 0{,}5\left((a_{20} - a_{02})^2 + a_{11}^2\right)^{1/2},\\ \theta &= 0{,}5 \operatorname{arctg}(a_{11}/(a_{20} - a_{02})).\end{aligned}\right\}$$

If the above-mentioned conditions for termination of the calculation are not fulfilled, the degree of the approximation polynomial is increased by 1 and the calculation proceeds according to formulas (3)-(7). The coefficients $a_{n,m}$ found in this way are revised in accordance with expression (1) and ultimately the coefficients of $W_{n,m}$ for the expansion of the real wave aberration in a Taylor series for the plane of best placement are obtained. The wave aberration can be simply calculated for any point in the pupil using the coefficients of $W_{n,m}$.

[illegible] was been developed into the INTERF [illegible] for this purpose we have provided for a supplementary call of INTERL, which searches for the optimal s here for comparison and interpolation by a locally linear method. We have also provided for linear and nonlinear correction of distorted interferogram scale.

Processing of the interferogram provides information on the phase composition of the pupil function $P(X_p, Y_p)$ in some cases (e.g. in optical systems operating with Gaussian laser beams and holographic optical elements). This information should be supplemented by the amplitude component of the pupil function $A(X_p, Y_p)$, when the overall function will have the form

$$P(X_p, Y_p) = A(X_p, Y_p) \exp(ikW(X_p, Y_p)),$$

where (X_p, Y_p) are normalized coordinates [10]. The pupil function is related to the point spread function and the optical transfer function by the well-known relationships [3]

$$\Phi PT(X, Y) = C_1 |F(P(X_p, Y_p))|^2; \quad (8)$$

$$OTF(\nu_X, \nu_Y) = C_2 F(\Phi PT(X, Y)), \quad (9)$$

where F is the two-dimensional Fourier transform operator, X and Y are the normalized coordinates in the image plane [11], ν_X and ν_Y are the normalized spatial frequencies in image space [11], and C_1 and C_2 are constant multipliers.

The calculation of the point spread function and the optical transfer function by (8) and (9) is carried out by the OTFDF subroutine using a fast Fourier transform (BPF). The use of the fast Fourier transform makes it possible to calculate the point spread function and the optical transfer function directly using the discrete Fourier trnasform, but satisfactory accuracy required storage and processing of large quantities of information which are not stored in the working memory of the computer. Accordingly we used magnetic drums to store the calculation results and certain intermediate data, but the interchange with the drum was organized in large blocks of information using the BAROBMEN subroutine system [11]. The Eklundh method was used for transposition of matrices, required in the performance of the two-dimensional Fourier transform [12]. The above enabled us to make full use of the advantages of the fast Fourier transform. The current variant of the program for the BESM-6 computer can calculate point spread function and optical transfer function matrices with sizes from 64 x 64 to 256 x 256 elements.

As an example we consider the processing of an interferogram of an astronomical objective with a pupil diameter of 500 mm obtained on an unequal-path laser interferometer for a point on the axis with $\lambda = 632$ nm.

Fig. 1 shows the distribution of wave aberrations with respect to the plane of best placement and Fig. 2 gives the results of calculation of the point spread function. Here the mean square value for wave aberration was 0.14 and the boundary values -0.65λ and $+0.38\lambda$, the effective astigmatism $A = 0.26\lambda$ and the Strehl number 0.5.

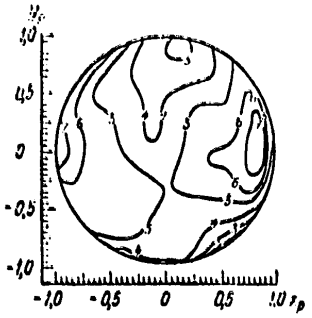

Fig. 1. Wavefront Contours (Distribution of Wave Aberration). X_p and Y_p are normalized coordinates on the screen. The contour interval corresponds to a wavefront difference of 0.125 λ .

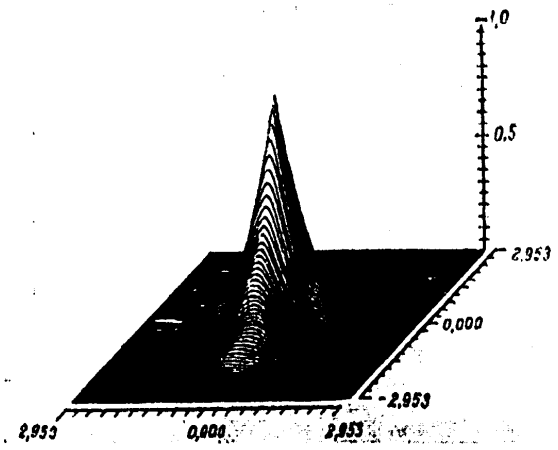

Fig. 2. The Point Spread Function (Normalized to the Strehl Number).

The results of calculation of the two-dimensional optical transfer function from the interferogram were compared with results from recording the modulus of the two-dimensional optical transfer function holographically obtained by P. A. Sergeyev and I. N. Tsvikevich. This method is based on holographic recording of the overall amplitude distribution in the image of a point and is analogous to the implementation of the digital method of computing the optical transfer function. The results of calculation of the modulus of the two-dimensional optical transfer function for an objective are shown in Fig. 3. Fig. 4 presents a graph of the moduli of the optical transfer function in the best and worst cross sections. As can be seen from the figures, the calculated and measured values agree with an accuracy of ± 0.03, which does not exceed the error of experimental determination of the modulus of the optical transfer function.

It should be noted in conclusion that contour maps of wave aberrations can be used to determine the areas and amounts of retouching; in addition, it is possible to determine the effectiveness of retouching by computer modeling.

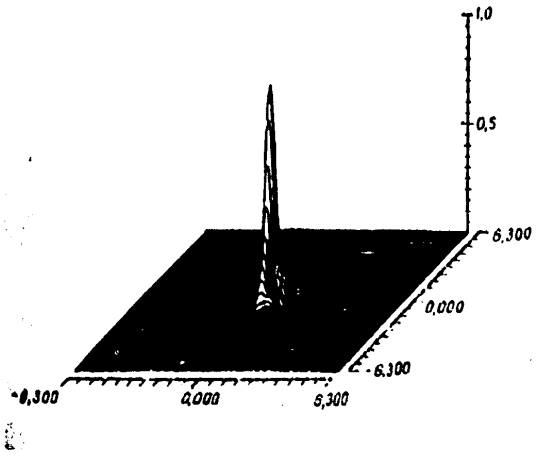

Fig. 3. The Modulus of the Optical Transfer Function.

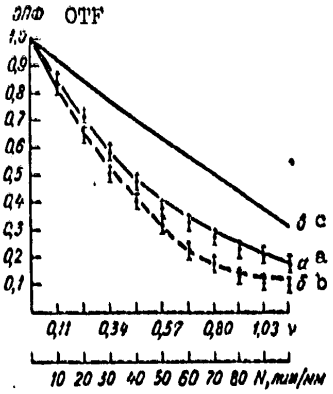

Fig. 4. Comparison of the results of calculation of the optical transfer function for real wave aberrations (Fig. 1) with data obtained by the holographic method: a is the modulus of the OTF in the best section, b is the modulus in the worst section, c is the modulus for a corresponding optical system without aberration. Broken lines represent calculated values, circles represent experimentally measured values.

BIBLIOGRAPHY

1. D. S. Volosov. Fotograficheskaya optika [Photographic Optics]. Moscow, Iskusstvo, 1971.

2. K. Preston. Coherent Optical Computers. Moscow, Mir, 1974.

3. M. Born; and E. Wolf. Fundamentals of Optics. Moscow, Nauka, 1970.

4. F. Twyman. PHIL. MAG., Vol 35, No 1 (1918), p 49.

5. G. Ivon. Metody kontrolya opticheskikh poverkhnostey [Methods of Testing Optical Surfaces]. Moscow, Leningrad, Oborongiz, 1939.

6. L. P. Moroz. OMP [Optiko-Mekhanicheskaya Promyshlennost'], No 11, 1936, pp 17-18; No 12, 1936, pp 14-16; No 1, 1937, pp 11-18.

7. V. A. Savin; and L. G. Fedina. Novaya tekhnika v astronomii [New Equipment in Astronomy], No 3. Leningrad, Nauka, 1970, pp 207-212.

8. I. M. Gel'fand. Lektsii po lineynoy algebre [Lectures on Linear Algebra], Moscow, Nauka, 1966.

9. D. Hudson. Statistics for Physicists. Moscow, Mir, 1970.

10. H. H. Hopkins. JAPAN JOURNAL OF APPL. PHYSICS. Vol. 4, No 1 (1965), pp 31-35.

11. V. I. Skripnichenko. Algoritmi nebesnoy mekhaniki [Algorithms of Celestial Mechanics]. Leningrad, 1974.

12. J. O. Eklundh. "IEEE", Vol 21, No 7 (1972), pp 801-803.

13. R. Berggren. OPTICAL SPECTRA, Vol 12 (1970), pp 22-25.

14. M. P. Rimmer; C. M. King; and D. G. Fox. APPL. OPT., Vol 11, No. 12 (1972), pp 2790-2796.

15. J. J. Bruhing et al. APPL. OPT., Vol. 13, No 1 (1974), pp 2693-2703.

Received 10 June 1977.

8480
CSO: 8144/0469

UDC 666.11.01:535.323

CATALOG OF OPTICAL GLASSES OF THE USSR AND GDR

Leningrad OPTIKO-MEKHANICHESKAYA PROMYSHLENNOST' in Russian No 9, 1978 pp 36-39

[Article by Corresponding Member of the USSR Academy of Sciences G. T. Petrovskiy, I. M. Buzhinskiy and Candidate of Sciences V. N. Polukhin]

[Text] The efforts to develop a joint USSR-GDR catalog of optical glasses are briefly characterized, their structure and content and the product range described, and the importance of the issuance of the catalog for current and future development of socialist integration in the optical glass field evaluated.

In keeping with the plan for scientific and technical cooperation between the USSR and the GDR in the area of optical glass making, in 1976 a catalog of optical glasses of the USSR and GDR was compiled and issued. The compilation of the joint catalog by the two largest producers of optical glass, each of which has its own long individual developmental history and traditions, is the first such experience in worldwide practice.

Compilation of the catalog required the solution during 1973-1976 of a complex of organizational, scientific and technical problems.

With the participation of a large number of specialists, the USSR-East German working groups solved the key problems, without a resolution of which it would have been impossible to compile a joint catalog of optical glasses. A unified system of norms for the main optical glass parameters was worked out and unified norm and reference values to be included in the catalog were established. Unified methods for testing the numerous glass parameters were found. We should note that at this stage the testing methods and apparatus could not be completely unified, but it was reliably demonstrated that in spite of the existence of differences they gave identical results in measurement of glass parameters. Unified quality requirements for optical glasses were determined and unified evaluation criteria adopted. The catalog listing, consisting of 238 glasses (an equal number for each of the two participants) was developed. The determination of the list was a complex problem, since it

was connected with established production of optical instruments on both sides and accordingly alterations in it could not always be made quickly where desired. Accordingly it was necessary to include in the catalog a large number of "duplicate" glasses; this is why the catalog is called "joint" and not "unified." Complete unification of the list is a future task, which will be intricate and prolonged.

The list of optical glasses was approved during compilation of the catalog: 25 new varieties of glass with extreme optical constants were incorporated, offering new possibilities for instrument making, and little-used and non-recommended glasses were eliminated. The glasses on the list are at the same level as those of the leading foreign companies, and in some cases surpass it. This catalog initiates the inclusion of not only optical glasses but also quartz glass, glass for fiber optics, and glass for bifocal eyeglasses with an invisible dividing line. Unified forms of supply were established and regulations for designation and coding of glasses coordinated.

In order to carry out these measures, the specialists on both sides conducted an immense amount of supplementary investigation of glass quality, testing of procedures, review, revision, updating and expansion of information on the physical and chemical properties of glasses, and also developed new procedures for investigating quality and rating properties.

During compilation of the catalog, the quality of optical glass was improved in a number of respects, including such important ones as light absorptivity and bubble content. A special section was devoted to specially pure glasses with light absorption coefficients of 0.1-0.3 percent per centimeter. Glass products with smaller tolerances and improved quality indices were included.

The joint catalog of USSR and GDR optical glasses is the most complete single modern reference work on optical glass. The extremely detailed text, includind a description of the catalog, appendices and also lists of the properties of each type of glass, gives the designer exhaustive information about the glass, its quality and the available forms, significantly simplifying the correct selection of glass and expanding the range of its applications.

The catalog gives for the first time refractive indices for all laser frequencies, provides a dispersion formula for calculating refractive indices for other wavelengths, and presents diagrams for the selection of pairs of glasses with minimal secondary spectral values in four wavelength regions:

$$[l-F(F')],\quad [g-F(F')],\quad [F(F')-e],\quad [F(F')-r]$$

along with complete data on the light transmissivity of domestic glasses (ordinary and high-transmissivity) for the entire spectrum.

The catalog gives 153 characteristics for each glass (the All-Union State Standard GOST 13859-68 gives 88).

Table 1.

USSR Glasses Стекла СССР

№ п/п	Марка 1 стекла	Кодовый 2 номер	n_d	ν_d	№ п/п	Марка 1 стекла	Кодовый 2 номер	n_d	ν_d
1	ЛК1 LK	001	1,43986	68,84	61	БФ21 BF	239	1,61413	40,03
2	ЛК3	002	1,48746	70,04	62	БФ24	242	1,63455	36,77
3	ЛК4	004	1,49037	65,12	63	БФ25	243	1,60772	46,11
4	ЛК6	007	1,47047	66,83	64	БФ26	245	1,63055	38,47
5	ЛК7	009	1,48287	66,33	65	БФ27	246	1,60682	43,97
6	ЛК8	011	1,47086	68,53	66	БФ28	248	1,66426	35,44
7	ФК11 FK	021	1,51997	69,14	67	БФ32	249	1,57941	46,69
8	ФК13	022	1,54687	67,60	68	ТБФ4 TBF	271	1,77878	38,08
9	ФК14	024	1,57998	65,08	69	ТБФ3	270	1,76586	41,15
10	ТФК1TFK	040	1,60848	65,22	70	ТБФ8	274	1,85850	36,64
11	К100	050	1,52158	59,62	71	ТБФ9	275	1,80847	42,77
12	К2	052	1,50047	56,02	72	ТБФ25	276	1,81239	37,45
13	К3	054	1,51007	63,36	73	ТБФ10	277	1,81481	33,42
14	К8	056	1,51637	64,07	74	ТБФ11	278	1,83277	43,08
15	К14	059	1,51478	60,63	75	ЛФ5 LF	296	1,57502	41,31
16	К15	061	1,53357	55,47	76	ЛФ7	298	1,67842	41,11
17	К18	063	1,51918	60,36	77	ЛФ8	299	1,55752	42,01
18	К19	064	1,51878	61,69	78	ЛФ9	300	1,58013	38,01
19	К20	066	1,52638	60,16	79	ЛФ10	301	1,54811	45,87
20	БК4 BK	081	1,53028	60,47	80	ЛФ11	302	1,56091	46,78
21	БК6	083	1,53998	59,67	81	ЛФ12	304	1,54021	44,87
22	БК8	085	1,54678	62,78	82	Ф1* F	316	1,61295	36,95
23	БК10	088	1,56889	56,05	83	Ф2	318	1,61655	36,61
24	БК13	093	1,55948	61,15	84	Ф4	320	1,62435	35,93
25	ТК2	107	1,57249	57,48	85	Ф6	322	1,60324	37,91
26	ТК4	109	1,61120	55,82	86	Ф9	327	1,61386	34,58
27	ТК8	111	1,61410	55,13	87	Ф13	329	1,62005	36,35
28	ТК9	113	1,61720	54,05	88	Ф18	331	1,62496	35,29
29	ТК12	115	1,56888	62,93	89	ТФ1 TF	341	1,64767	33,87
30	ТК13	117	1,60389	60,63	90	ТФ2	344	1,67268	32,23
31	ТК14	119	1,61309	60,58	91	ТФ3	345	1,71741	29,51
32	ТК16	121	1,61269	58,35	92	ТФ4	347	1,74002	28,16
33	ТК17	124	1,62800	59,36	93	ТФ5	349	1,75523	27,53
34	ТК20	125	1,62210	56,71	94	ТФ7	351	1,72822	28,34
35	ТК21	127	1,65691	51,12	95	ТФ8	353	1,68949	31,13
36	ТК23	129	1,58919	61,24	96	ТФ10	355	1,80627	25,37
37	СТК3 ST	166	1,65950	57,35	97	ТФ11	357	1,64878	31,59
38	СТК7 STK	168	1,68701	53,59	98	ТФ12	358	1,78517	25,67
39	СТК8	169	1,70313	49,69	199	ТФ13	359	1,78466	26,33
40	СТК9	170	1,74253	50,24	100	СТФ2 STF	366	1,94449	20,42
41	СТК10	172	1,73794	48,11	101	СТФ3	367	2,17018	17,03
42	СТК12	174	1,69201	55,01	102	СТФ11	368	2,05624	16,63
43	СТК15	176	1,70931	54,77	103	ОФ1 OF	386	1,52949	51,81
44	СТК16	177	1,78595	45,62	104	ОФ3	389	1,61242	44,09
45	СТК19	178	1,74413	50,42	105	ОФ4	390	1,65063	43,46
46	СТК20	180	1,76482	50,25	106	ОФ5	391	1,66264	41,78
47	ОК1	191	1,52226	76,35	107	ОФ6	392	1,60121	51,04
48	ОК2	193	1,55027	73,08	108	КУ1 KU	750	1,45816	67,84
49	КФ4 KF	202	1,51818	58,95	109	КУ2	751	1,45846	67,84
50	КФ6	205	1,50058	57,21	110	КВ KV	752	1,45846	67,84
51	КФ7	207	1,51759	51,15	111	КИ KI	753	1,45846	67,84
52	БФ1 BF	217	1,52479	54,95	112	КВ-Р KV-R	754	1,45846	67,84
53	БФ4	219	1,54809	53,95	113	ББК3 BBK	774	1,5210	57,8
54	БФ6	221	1,56970	49,45	114	БОК1 BOK	770	1,5220	58,7
55	БФ7	223	1,57960	53,87	115	БОФ2 BOF	771	1,6247	35,7
56	БФ8	225	1,58271	46,47	116	ВС682 VS	853	1,68243	52,57
57	БФ11	227	1,62231	53,14	117	ВС586	854	1,58592	41,20
58	БФ12	229	1,62604	39,10	118	ВС513	862	1,51311	64,54
59	БФ13	231	1,63962	48,27	119	ВС488	863	1,48806	65,51
60	БФ16	233	1,67103	47,29	120	ЛК5 LK	005	1,47817	65,59

Key: 1. Variety 2. Code number

Table 2.

GDR Glasses Стекла ГДР

№ п/п	Марка стекла [1]	Кодовый номер [2]	n_d	ν_d	№ п/п	Марка стекла [1]	Кодовый номер [2]	n_d	ν_d
1	FK3	013	1,46450	65,67	60	BaF3	356	1,58266	46,52
2	FK5	016	1,48749	69,99	61	BaSF5	357	1,60323	42,50
3	PSK1	043	1,54771	62,53	62	BaF4	358	1,60562	43,91
4	PSK3	044	1,55232	63,49	63	BaF5	359	1,60729	49,31
5	PSK2	045	1,56871	63,05	64	BaF7	360	1,60801	46,20
6	BK9	058	1,49386	66,07	65	BaF	362	1,61952	49,10
7	BK3	059	1,49829	65,14	66	BaF8	364	1,62374	47,00
8	BK7	064	1,51666	64,06	67	BaF9	365	1,64028	47,80
9	BK6	066	1,53114	62,12	68	BaF10	367	1,67004	47,18
10	BK7	068	1,51667	64,06	69	KzF1	383	1,55115	49,60
11	K11	101	1,50013	61,50	70	KzFS2	384	1,55781	53,84
12	K10	102	1,50136	56,46	71	KzFS1	386	1,61306	43,98
13	K1	104	1,50976	61,86	72	KzF3	388	1,52411	53,10
14	K3	107	1,51622	58,99	73	KzF6	381	1,52683	51,12
15	K13	109	1,52246	59,11	74	LaF	401	1,69712	46,97
16	K14	110	1,52421	58,62	75	LaF	402	1,73111	46,32
17	K14	113	1,52421	58,58	76	LaF	409	1,77013	40,76
18	ZK7	124	1,50851	61,05	77	LaSF	423	1,82778	30,09
19	ZK2	127	1,52068	60,13	78	LaSF	424	1,83988	28,37
20	ZK1	128	1,53316	58,01	79	LF7	457	1,57502	41,33
21	ZK5	129	1,53373	55,13	80	LF3	460	1,58214	42,03
22	BaLK2	142	1,51783	61,04	81	F8	474	1,59550	39,22
23	BaK2	155	1,53996	59,63	82	F16	475	1,59944	35,40
24	BaK5	156	1,55670	58,57	83	F5	477	1,60137	38,15
25	BaK4	158	1,56884	56,00	84	F3	479	1,61292	36,96
26	BaK1	159	1,57248	57,45	85	F4	480	1,61659	36,64
27	BaK4n	162	1,56884	56,02	86	F2	481	1,62006	36,35
28	SK11	171	1,56385	60,72	87	F11	482	1,62009	35,95
29	SK5	173	1,58912	61,29	88	F7	485	1,62535	35,59
30	SK13	174	1,59182	58,23	89	BaSF3	501	1,60717	40,26
31	SK14	175	1,60352	60,96	90	BaSF1	503	1,62605	39,08
32	SK2	177	1,60738	56,71	91	BaSF4	504	1,65130	38,35
33	SK4	181	1,61273	58,63	92	BaSF9	505	1,66083	41,54
34	SK6	183	1,61376	56,30	93	BaSF2	506	1,66146	35,89
35	SK9	184	1,61406	55,17	94	BaSF6	507	1,66755	41,94
36	SSK4	185	1,61766	55,12	95	BaSF7	508	1,70155	41,16
37	SK16	186	1,62042	60,26	96	BaSF8	509	1,72343	38,01
38	SK15	187	1,62299	58,13	97	SF7	520	1,63978	31,62
39	SK10	188	1,62280	56,87	98	SF2	522	1,64769	33,87
40	SK18	189	1,63853	55,56	99	9	524	1,65504	33,39
41	SK24	203	1,66359	56,41	100	19	525	1,66681	33,10
42	SK22	204	1,67807	55,00	101	5	526	1,67270	32,24
43	SSK10	205	1,69341	53,56	102	8	527	1,68893	31,15
44	SSK11	229	1,75300	53,11	103	15	528	1,69895	30,06
45	SSK1	263	1,61719	54,05	104	1	529	1,71736	29,50
46	SSK7	265	1,61848	50,35	105	10	530	1,72824	28,35
47	SSK2	266	1,62229	53,14	106	3	531	1,73998	28,16
48	SSK5	267	1,65843	50,86	107	13	532	1,74076	27,71
49	LLF8	284	1,53304	45,15	108	4	533	1,75520	27,53
50	KF3	301	1,51454	54,66	109	SF14	534	1,76184	26,53
51	KF8	307	1,51116	50,96	110	SF11	535	1,78473	25,73
52	BaLF5	319	1,54740	53,61	111	SF6	536	1,80516	25,46
53	BaLF1	321	1,56248	50,89	112	SFS1	537	1,92286	20,95
54	BaLF3	322	1,57134	53,00	113	Q1	871	1,45851	67,80
55	BaLF4	324	1,57957	53,90	114	Q2	872	1,45851	67,80
56	BaLF9	327	1,59306	51,93	115	Q3	873	1,46851	67,80
57	LLF6	338	1,53171	48,90	116	SQ1	878	1,45816	67,83
58	LLF2	339	1,54072	47,25	117	D1	933	1,63867	34,74
59	LLF7	341	1,54869	45,41	118	KLF	382	1,52914	51,78

Key: 1. Variety 2. Code number

The text of the catalog includes the following sections, which give scientific descriptions of the determining properties of glasses: optical constants, transmissivity and scattering, chemical stability, temperature characteristics, mechanical properties, electrical and magnetic properties, quality indicators, forms of availability, test logs, lists of data on properties (an individual list for each variety), diagrams of glass types and the characteristic dispersion curve for the spectrum.

The appendices give tables of reflectivities as a function of refractive index, nomograms for determining the internal transmissivity and the overall transmissivity from the light absorption coefficient; tables of coefficients for converting the measurement units used in the catalog into the international system of units, and geometric dimensions and tolerances for various available shapes (Appendices S1 and D1); changes in the list of glasses of codes S and D (Appendices S2 and D2); optical quartz glass (Appendices S3 and D3); optical glass for fiber optics (Appendices S4 and D4); optical glass for eyeglasses (Appendices S5 and D5); and high-transmissivity optical glass (Appendices S6 and D6).

The catalog is compiled in two languages and printed in two identical variants: variant S, in which the description begins with the Russian text, and variant D, in which it begins with the German text. The designations of the catalog are: complete catalog; version S, OS1; version D, OD1. A list of the glasses included in the joint catalog is given in Tables 1 and 2.

In the opinion of specialists on both sides, the catalog is a document of great importance for the further development of optical glass and optical glass making and an example of successful implementation in practice of socialist integration.

Even during the preparatory stages, optical and mechanical experts on both sides made successful use of new optical glasses included in the joint catalog in the development of new optical systems.

The introduction of this catalog will make it possible to improve the quality of optical-mechanical instruments as the designers use higher-quality glasses, and will lead to greater specialization and extent of socialist integration, and as a result higher output and greater quality of optical glass.

Interested organizations may obtain the joint catalog of USSR and GDR optical glasses from the House of Optics in Moscow.

Received 10 March 1978.

8480
CSO: 8144/0469

UDC 666.1;621.375.9:535

MECHANICAL STRENGTH AND THERMAL STABILITY OF NEODYMIUM GLASSES

Leningrad OPTIKO-MEKHANICHESKAYA PROMYSHLENNOST' in Russian No 9, 1978 pp 39-42

[Article by V. M. Mit'kin, Candidate of Sciences O. S. Shchavelev and V. B. Zheltov]

[Text] The results of a study of maximum stresses of the lateral surfaces of active elements and comparison of these data with thermal stabilities are presented. It is shown that the mechanical strength of phosphate glass specimens is within the 150-300 kg/cm^2 range and that for silicate glasses in the 300-600 kg/cm^2 range. The thermal stability of optical glasses of various chemical compositions is studied. A method for evaluating the thermal stability of glasses from their composition and coefficient of thermal expansion is presented.

Neodymium glass, which is used in laser engineering for the manufacture of active elements, has been an object of study for some time. Investigations which were limited to questions of spectroscopy, thermal optics and manufacturing processes have resulted in the development of extremely promising glasses [1, 2]. Further possibilities for the use of neodymium glasses in laser engineering depend to a significant degree on the problem of their mechanical strength and thermal stability [3]. However, the literature contains insufficient information about these properties.

We shall discuss the results of studies of thermal stability and maximum stress on the lateral surface of cylindrical active elements and data on the dependence of the thermal stability of optical glass on its chemical composition.

In contrast to the classical methods of breaking of samples (tensile testing, bending, impact and so on) we created mechanical stresses in the active elements while they were in the laser head by optical pulping (internal heating) and intense cooling of the lateral surfaces with liquid (see e.g. [4]). This produces a quasi-stationary parabolic temperature distribution across the active element as the pumping pulses are periodically applied, resulting in stresses with a similar radial distribution in the material [5]. The maximum

stresses occur at the center (compression) and on the lateral surface (extension). Tensile stresses on the lateral surface result in breaking when the maximum value is exceeded. In the method employed by us, the stress on the surface of the sample is uniquely determined by the frequency of the pump pulses and is monitored through a conoscopic pattern observable when the sample, located between crossed polarizers, is illuminated. For calculating the stress on the lateral surface of the cylindrical sample we used a formula with rather wide approval in quenching technology [6, 7]:

$$\sigma_{\text{пов}} = 2\frac{n\lambda}{lB}; \qquad (1)$$

where n is the number of rings in the conoscopic pattern; λ is the wavelength of the illumination source; l is the length of the sample; and B is the optical load coefficient.

It is well known that the strength and durability of any glass sample depend on the condition of its lateral surface and depend in practice on the presence or absence of microcracks. A temperature fluctuation mechanism correctly explains breaking [8]. The actual strength of a glass sample is considerably lower than the theoretical strength determined from the strength of the glass structure [8], i.e. glass breaks before the yield point is reached as a result of defects in the lateral surface [8]. This circumstance and the fact that the radial stress distribution in quenched samples and the samples described above are identical (this is shown experimentally in reference [4] by mutual compensation of stress) enabled the authors to use formula (1) to calculate the stress σ_{max} resulting in breaking of the sample. For this purpose we determined the number of rings n_{max} in the conoscopic pattern before breaking of the sample and substituted the value into formula (1). The values for the breaking strengths thus obtained for active elements with a diameter of 10 mm and a length of 130 mm with an etched lateral surface are presented in Table 1. The error in the values for σ_{max} which were found results primarily from error in measurement of the number of rings n_{max}, which amounts to about ± 0.5 and ± 1 respectively for a small (approximately 5) and large (⩾ 10) number of rings.

Table 1.

	1 Марка стекла	2 $\sigma_{пред}$, кг/см²	3 $\Delta T_{эксп}$, °C Ø 10 × × 130 мм	4 $\sigma^{*}_{пред}$, кг/см²	5 $\sigma^{**}_{пред}$, кг/см²
GLS	ГЛС1	520±40	89	560±10	550
	ГЛС3	460±40	79	470±10	490
LGS	ЛГС250-3	430±40	76	450±10	470
KGSS	КГСС8Т	390±20	55	395±10	340
	КГСС1621	220±20	37	205±10	230
	КГСС9199	160±20	33	180±10	200

Key: 1. Glass variety
2. σ_{max}, kg/cm² [maximum stress]
3. $\Delta T_{exper.}$
4. σ^{*}_{max}, kg/cm² [maximum stress calculated from formula (3)]
5. σ^{**}_{max}, kg/cm² [maximum stress calculated from formula (4)]

For systematic study of the thermal stability of glasses as a function of their composition we used etched samples with dimensions of 9.5 x 9.5 x 61 mm with a 1-mm bevel on the edges, manufactured from 31 industrial and experimental optical and neodymium glasses which differed from commercial glass, whose thermal stability is rather well studied (see e.g. [6]) by a high volume homogeneity of physical and chemical properties and an extremely broad range of chemical compositions based on different glass-formers (e.g. phosphate, silicate and so on). The samples were cut from highly homogeneous bubble-free pieces of glass. After polishing with M12 powder for silicate and M5 powder for phosphate glasses, the samples were etched to decrease the number and the amount of danger from defects and to distribute them evenly over the entire surface. The above was aimed at decreasing the difference in homogeneity of properties between samples of a single variety of glass, which plays a significant part in the dispersion of experimental thermal stability values (for example, the great dispersion of thermal stability of samples of non-homogeneous technical glasses). The initial measurements taken on a large number of samples of the glasses KGS51621 and GLS1 (38 and 33 samples respectively) indicated that as a result of the above measures, the dispersion of thermal stability values for different samples of the same variety of glass was extremely small (no greater than 2-4° C), making it possible in subsequent experiments to limit ourselves to 10 specimens of glass of each variety, or even to five in a few cases (it must be noted that the dispersion of values for each variety of glass did not exceed the value indicated). The thermal stability was determined by dropping samples heated in a special furhace into water at room temperature. Before dropping into the water, the samples were held at each temperature for 20 minutes. Near the expected maximum loads, the furnace temperature was increased by 2-degree increments between trials until all samples had broken. In design, our unit differed from the standard unit used in determining the thermal stability of commercial glasses [9] only in the dropping mechanism.

The experimental thermal stability values ΔT in Fig. 1 were compared with the values for the coefficient of thermal expansion α for the glass in the temperature interval 20-120° C using measurements obtained by the interference method. Although the nature of the relationship $T = f(\alpha)$ for optical glasses in general is similar to the relationship given in the literature for commercial glasses [9], the presence of glasses from five different chemical composition groups was clearly observable; for these glasses the relationship can be written using linear equations with different coefficient values (Table 2):

$$\Delta T = \Delta T_0 - \frac{d(\Delta T)}{d\alpha}, \qquad (2)$$

where ΔT_0 is the thermal stability of a hypothetical glass with $\alpha = 0$; and $d(\Delta T)/d\alpha$ is the angular coefficient of change of thermal stability. The thermal stability of glass samples is calculated from equation (2) with almost the same accuracy as the experimental determination.

For glasses in the first group, including borosilicates with a coefficient of thermal expansion not greater than $50 \cdot 10^{-7}$ deg^{-1}, the thermal stability decreases sharply as the coefficient of expansion increases. The glasses in the other groups also showed decreased ΔT as the coefficient of thermal expansion increased, but they had a practically identical value for the coefficient

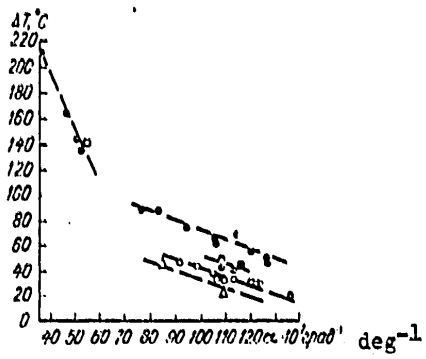

Fig. 1. Relationship of Thermal Stability of Optical Glasses to Coefficient of Thermal Expansion.

●-Borosilicates; ● alkali silicates; □ alumoborate-silicates; ◌ calcium phosphates; ■ calcium-strontium phosphates; ○ barium and lead phosphates; ◌ alumofluorophosphates; △ polylead silicates.

$d(\Delta T)/d\alpha$, about one-sixth that for borosilicate glasses in the first group. Accordingly glasses have different thermal stabilities for the same coefficient of thermal expansion. This coefficient is highest for the alkali silicate group. Among phosphate glasses, those with calcium oxide are the most thermally stable. Barium-phosphate, lead-phosphate and fluorophosphate glasses are less thermally stable than calcium-phosphate glasses. The lowest thermal stability is observed for multi-lead silicate glasses. The thermal stability levels for glasses in the four latter groups differ by approximately 20° C.

The thermal stability of active elements 130 mm long made of a number of industrial neodymium glasses were determined as a function of their diameters within the range 5-15 mm. The relationship of ΔT to the diameter d which was obtained is shown in Fig. 2, and for samples of 10 mm diameter also in Table 1. The figure shows that the thermal stability of samples decreases as their diameters increase. Here in order to obtain a straight line we also included points corresponding to the thermal stability of samples with square cross sections which were used for systematic studies, taking the maximum cross-sectional dimension (the diagonal) as the diameter. The extent of the decrease in thermal stability in a rod of silicate glass as the diameter decreases by a millimeter averages 5.2 degrees, and that for phosphate glasses 2.7 degrees. The divergence of these values within the groups studied did not exceed 1 deg/mm.

The thermal stability values which we obtained for neodymium glasses agree well with the data of other authors [10]. We used them to calculate the maximum stress in rods 10 mm in diameter x 130 mm by the well-known formula:

$$\sigma^{\bullet}_{\text{пред}} = \frac{\alpha E}{1-\mu}\,\Delta T\,\text{Bi}\,S_m, \qquad (3)$$

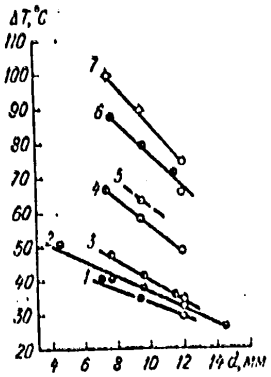

Fig. 2. Thermal Stability of Neodymium Glasses as a Function of Diameter

Phosphate glasses:
1. KGSS9199
2. GLS22
3. KGSS165h

Silicate glasses:
4. KGSS8T
5. GLS253-2
6. GLS3
7. GLS1

where E is Young's modulus; μ is the Poisson coefficient; and BiS_m is a coefficient depending on the intensity of heat withdrawal and the shape of the specimen [5]. The values of BiS_m in the function for Biot's criterion characterizing the intensity of heat removal from the lateral surface of the sample for rod-shaped samples with circular (curve 2) and rectangular (curve 1) cross section are shown in Fig. 3 (data from reference [6], supplemented by the authors for cylindrical samples). Under the experimental conditions, $BiS_m \approx 0.65$. The results of calculating σ^*_{max} are shown in Table 1. There is good agreement with the values of σ_{max}, thus indirectly confirming the suitability of the method presented above for finding maximum stress.

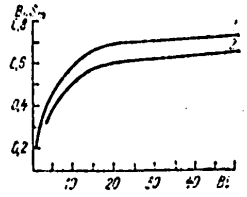

Fig. 3

The connection between the tensile stress on the lateral surface of the sample and its thermal stability can be described not only by the formula given above, but also by a simpler formula obtainable by substituting in (1) the double refraction value $n_{max}\lambda = Q\alpha\Delta T$:

$$\sigma^{**}_{пред} = 2\frac{Q}{B}\Delta T, \qquad (4)$$

where Q is the thermooptical characteristic of the glass as given in [2]. The calculated values σ^{**}_{max} are given in Table 1; an average value Q/B = 3.1 for the glasses was used in the calculation.

Thus the investigation establishes that the mechanical strengths of the samples of neodymium phosphate glass are in the 150-300 kg/cm^2 range and those for the neodymium silicate glass samples in the 350-600 kg/cm^2 range. The breaking stress may be calculated rather accurately from the thermal stability of the sample. It may be found relatively easily by experiment or estimated from the composition of the glass and adjusted for the diameter of the sample.

In conclusion we note that the stresses withstood by the glass samples depended on the time of heating [11]. The maximum load values were greater when this was short. Fig. 4 shows the change in breaking stress on the lateral surface of a sample 10 mm in diameter by 130 mm long of GLS1 glass as a function of the heating time t. The value σ^*_{max} determined from the thermal stability corresponds to small t. The relationships obtained are described by the well-known formula [11]

Here t is the durability of the sample and A and K are constants of the material which depend on the temperature.

Table 2.

a Номер группы	b Группа стекол	c Содержание основных компонентов, вес. %	ΔT_0,	$d(\Delta T)/d\tau$, 10^7 град$^{-2}$ deg^{-2}
1	боросиликатная	SiO_2 до 80 B_2O_3 до 40 Al_2O_3 до 20 R_2O до 10	359	−4,2
2	щелочносиликатная	SiO_2 50–70 RO до 20 R_2O 7–25 B_2O_3 до 20 R_2O_3 до 10	143	−0,7
3	кальциевофосфатная	P_2O_5 55–75 CaO до 10 R_2O до 10 R_2O_3 до 10	120	−0,68
4	барневосвинцовофторфосфатная	P_2O_5 40–50 BaO 10–40 PbO до 45 R_2O до 5 R_2O_3 до 10 до 65	108	−0,68
5	многосвинцовосиликатная	SiO_2 до 20 PbO 75–85	101	−0,7

Key: a. Group number
b. Group
c. Content of main components, % by weight

1. Borosilicate
2. Alkali silicate
3. Calcium phosphate
4. Barium-lead fluorophosphate
5. Polylead silicate

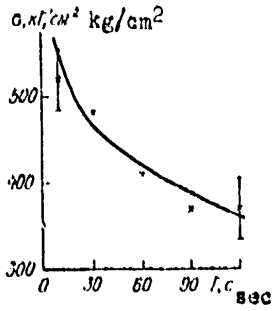

Fig. 4. Effect of Duration of Heating on Sample Durability

Key: x: experimental values
Solid line: curve calculated from formula (5)
Assumed values: A = 30,000, K = 0.0148

BIBLIOGRAPHY

1. M. M. Bubnov et al. KVANTOVAYA ELEKTRONIKA, No 4 (16), 1973, p 113.

2. O. S. Shchavelev et al. OMP [OPTIKO-MEKHANICHESKAYA PROMYSHLENNOST'], No 7, 1976, p 32.

3. A. A. Mak et al. KVANTOVAYA ELEKTRONIKA, Vol 2, No 4, 1975, p 850.

4. V. M. Mit'kin. OMP, No 8, 1976, p 26.

5. B. R. Belostotskiy; and A. S. Rubanov. Teplovoy rezhim tverdotel'nykh OKG [The Thermal Regime of Solid-State Lasers]. Moscow, Energiya, 1973.

6. G. M. Bartenev. Mekhanicheskyye svoystva i teplovaya obrabotka stekla [Mechanical Properties and Thermal Treatment of Glass]. Moscow, Stroyizdat, 1960.

7. I. A. Boguslavskiy. Vysokoprochnyye zakelennyye stekla [High-Strength Tempered Glasses]. Moscow, Stroyizdat. 1969.

8. G. M. Bartenev. Sverkhprochnyye i vysokoprochnyye neorganicheskyye stekla [Super-Strength and High-Strength Inorganic Glasses]. Moscow, Stroyizdat, 1974

9. H. Schonborn. J. SOC. GLASS TECHN., Vol 20, 1936, p 81.

10. I. M. Buzhinskiy; and S. K. Mamonov. TRUDY MVTU, Vol 184, 1974, p 181.

11. A. Ya. Bokin. Mekhanicheskyye svoystva silikatnykh stekol [Mechanical Properties of Silicate Glasses]. Leningrad, Nauka, 1970.

Received 21 June 1977.

8480
CSO: 8144/0469

UDC 539.234

WIDE-BAND DIELECTRIC MIRRORS MADE OF TITANIUM AND SILICON DIOXIDES

Leningrad OPTIKO-MEKHANICHESKAYA PROMYSHLENNOST' in Russian No 9, 1978 pp 46-47

[Article by L. L. Matskevich, V. V. Bazhinov and N. V. Ruchinskiy]

[Text] A method of producing broad-band dielectric merrors for the 0.4-1.0 micron range from TiO_2 and SiO_2, in which the TiO_2 is applied by reactive evaporation of TiO, is described. Graphs of the spectral transmission of 17-, 21- and 33-layer mirrors are presented.

Currently it is mainly ZnS and flourides [1-3] which are used to produce broad-band dielectric mirrors with a reflectivity above 90 percent, but these mirrors have low operating characteristics. The process of application of the refractory oxides SnO_2, ZrO_2 and SiO_2 by electron-beam evaporation in a vacuum [4] which has recently been developed does not solve the problem of manufacturing broad-band mirrors, owing to the low refractive indices of SnO_2 and ZrO_2 films. By resistive evaporation of titanium and silicon monooxides in oxygen [5] it is possible to produce two-oxide films of these substances with satisfactory refractive indices. But this method is very labor-consuming in the manufacture of mirrors with large numbers of layers.

We have demonstrated the possibility of producing beam-splitting and reflective surfaces with TiO_2 films by reactive evaporation of titanium oxides [6]. Using the process of reactive evaporation of TiO_2 we produced broad-band dielectric mirrors for the 0.4-1.0 micron range. The coatings were applied to a substrate of K8 glass, either unheated or heated to 350-400° C. The refractive indices of the titanium dioxide films were determined spectrophotometrically [7].

The films applied to the unheated substrate have a refractive index of 2.15-2.2 in the visible portion of the spectrum. Studies conducted since the conclusion of the work presented in [6] have indicated that the refractive indices obtained for titanium dioxide films depend on the quantity of the starting substance (TiO) evaporated, i.e. the chemical composition of the substance in the electron-beam evaporation crucible, which tends to have an increasing oxygen content, so that the refractive index of the TiO_2 film increases. The change

in chemical composition of the material in the crucible can be observed visually, since after the TiO has been heated in the crucible for 30-40 minutes in the presence of oxygen ($\sim 5 \cdot 10^{-4}$ mm of mercury) the yellowish-brown TiO is converted into a mixture of blue-violet higher oxides (Ti_2O_3, Ti_3O_5 and so on). When these higher oxides are exaporated, TiO_2 films with refractive indices of 2.15-2.2 are obtained. The refractive indices of TiO_2 films applied to a substrate heated to 350-400° C are 2.6-2.65 in the visible range and decrease to 2.45 at a wavelength of 1.0 microns.

The broad-band mirrors were prepared from two oxides, titanium and silicon dioxides. Both materials were evaporated by an electron beam evaporator. The mirrors consisted of several elementary quarter-wave mirrors with intermediate reflective bands [1, 2]. The mirrors all had the same design:

$$\begin{matrix} & \lambda_1 & & \lambda_2 & & \lambda_3 & & \lambda_4 & & \lambda_5 \\ S & (BH\ldots B) & H & B & H & (BH\ldots B) & H & B & H & (BH\ldots B) \\ & 11 \text{ layers} & & & & 9 \text{ layers} & & & & 7 \text{ layers} \end{matrix}$$

(33-layer mirror on heated glass substrate)

Here S is the substrate, K8 glass; B is the TiO_2 layer, with a thickness of $\lambda/4$; H is the SiO_2 layer, with a thickness of $\lambda/4$; λ_1, λ_3 and λ_5 are the wavelengths for which the optical thicknesses of the 7-, 9- and 11-layer were controlled; and λ_2 and λ_4 are the wavelengths for which the optical thicknesses of the intermediate layers were controlled; λ_2 and λ_4 had values intermediate between λ_1 and λ_3 and λ_3 and λ_5 respectively. A TiO_2-SiO_2 system consisting of 21 layers (see figure, graph a, curve 1) was applied to the unheated substrate.

The integral reflection was measured with a selenium photoelement with a correcting light filter made of ZS8 and ZhZS18 colored glasses; for the mirror in question it was 93.5% with a transmissivity of 5.6%. The accuracy of measurement of the transmissivity and reflectivity was 0.1% and 0.2% respectively. The light scattering, measured with a YuS-36, was 0.13%.

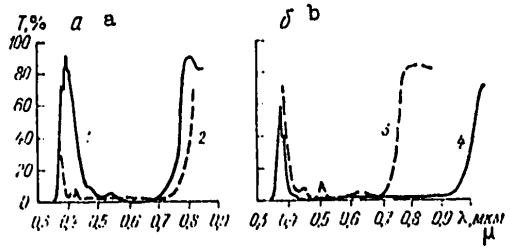

Spectral Curves of Transmissivity of Dielectric Mirrors

Key: a: curves 1 and 2 are for 21-layer mirrors on cold and heated substrates respectively.
b: curves 3 and 4 are for 17- and 33-layer mirrors on a heated substrate.

A series of mirrors consisting of 17, 21 and 33 layers were prepared on heated substrates. The integral mirror characteristics are shown in the table and the spectral characteristics are given in the figure.

1 Количество слоев	17	21	33
2 Интегральный коэффициент отражения, %	91,0	95,5–97,0	97,5–98,0
3 Интегральный коэффициент рассеяния, %	0,12–0,13	0,11–0,16	0,28–0,30

Key; 1. Number of layers
2. Integral reflectivity, %
3. Integral coefficient of scattering. %

The moisture resistance of the mirrors prepared on both the cold and heated substrates was evaluated by holding them in a climatic chamber (temperature 40° C, relative humidity 98%) and in running water. After 10 hours in the chamber, none of the mirrors studied had changed its mechanical strength or optical characteristics.

Thus moisture-resistant and and mechanically strong broad-band mirrors based on TiO_2-SiO_2 applied to heated and unheated substrates have been prepared using the vacuum method.

From analysis of the relatively high scattering coefficients of the mirrors we may conclude that these values are primarily determined by the number of layers in the system rather than by the high temperature of the substrate. In addition, the scattering level in the TiO_2 layers is significantly lower than in layers manufactured by the cathode [8] or high-frequency [9] methods, with comparable optical and mechanical characteristics. This attests to the advantages of the reactive method of producing the TiO_2 layers. The search for ways of decreasing the light scattering will continue.

BIBLIOGRAPHY

1. F. A. Korolev et al. OPT. I SPEKTR., Vol 28, 1970, p 775.

2. A. F. Turner; and P. W. Baumeister. APPL. OPT., Vol 5, 1966, p 69.

3. D. L. Perry. APPL. OPT., Vol. 4, 1965, p 987.

4. A. F. Perveyev; E. I. Fadeyeva; and G. A. Muranova. OMP [OPTIKO-MEKHANICHESKAYA PROMYSHLENNOST'], No 11, 1973, p 66.

5. V. N. Rozhdestvenskiy; and E. I. Fadeyeva. OMP, No 12, 1975, p 44.

6. L. L. Matskevich; and V. V. Bazhinov. OMP, No 2, 1977, p 41.

7. G. Khass; and R. Tun. The Physics of Thin Films. Moscow, Mir, 1977, p 136.

8. O. A. Motovilov; and O. G. Rudina. OMP, No 6, 1974, p 36.

9. A. F. Perveyev et al. OMP, No 3, 1975, p 43.

Received 18 December 1977.

8480
CSO: 8144/0469

UDC 531.717.8:778.38

MEASURING RADII OF CURVATURE AND LOCAL DISTORTIONS OF MIRROR SURFACES

Leningrad OPTIKO-MEKHANICHESKAYA PROMYSHLENNOST' in Russian No 9, 1978 pp 56-58

[Article by M. L. Gurari, A. P. Golikov and S. I. Prytkov]

[Text] Radii of curvature and local distortions of optical mirror surfaces are measured without using high-quality optics by the holographic shearing interferometer, whose size does not depend on the curvature of the mirror being studied.

The problem of accurate measurement of radii of curvature and defects of shape in the surfaces of mirrors in optical components using interference methods [1] becomes much more difficult as the dimensions and radii of curvature of the mirrors increase.

The contact interferometric methods which are in broad use under production conditions (e.g. the test glass method) produce greater errors as the dimensions of the mirrors increase, necessitating frequent readjustment of the etalon.

In non-contact interference instruments, such as the Twyman-Green unequal-path interferometer [2], shear interferometers or scatter-screen interferometers [3-6], the base of the measuring device typically depends on the radius of curvature of the mirror being tested, so that the possibility of testing large mirrors with increasing radii of curvature is limited by the increasing role of vibration, air currents and the like. Testing of convex mirrors under similar conditions requires large-diameter matching objectives, whose precision manufacture is troublesome.

The possibility offered by holographic interferometry of comparing wavefronts of any form recorded at different moments of time has made it possible to develop a method of precise measurement of radii of curvature and surface shapes of large mirrors using a device of relatively small dimensions and independently of the value or sign of the radius of curvature of the mirrors.

A schematic of the measuring device is given in Fig. 1. The mirror to be tested is mounted on a movable dolly, enabling it to be gradually moved along or perpendicular to the optical axis or to be turned relative to the apex. A diffuser, covering the aperture of the mirror to be tested, is placed before the mirror at as small a distance as possible. The main requirement for the diffuser is that the intensity of diffusion of the scattered component of the radiation be less that the intensity of the wave passing through it without scattering. The mirror is illuminated through the diffuser by a divergent beam from a coherent point source located on the optical axis of the mirror. The radiation reflected from the mirror passes through the diffuser in the reverse direction, falls on a photographic plate and serves as the object beam in the recording of the hologram. The entire unit is mounted on an anti-vibration platform whose dimensions are determined primarily by the requirement of optimal illumination and coverage of the mirror by the diffuser.

While the hologram is being produced, the photo plate is not moved from its exposure position. The diffuser surface is viewed through the hologram that has been obtained. The mirror being tested is moved from its initial position, producing an interference pattern located in the plane of the diffuser and recordable behind the hologram. The shape and period of the fringes in the interference pattern contain information about the radius of curvature and the shape of the mirror surface.

The observable interference pattern is produced primarily by the component of the initial illuminating beam which passes through the diffuser without scattering, is reflected from the mirror surface and is scattered as it passes back through the diffuser. Two such waves are observed simultaneously: one is recorded on the hologram, and the other is observed directly and corresponds to the mirror in its shifted position. It can be shown that the observable pattern is equivalent to the interference pattern in the diffuser produced by waves from two identical sources: images of the illumination source in the mirror in the initial and shifted positions. During testing of a spherical mirror this pattern has the form of equidistant straight lines with a period

$$\delta = \frac{\lambda}{\Delta}\left[\frac{R}{2} + \frac{z_q}{z_s}\left(\frac{R}{2} - z_s\right)\right],$$

where Δ is the size of the transverse shift (perpendicular to the axis) of the mirror, R is the radius of curvature of the mirror, and z_q and z_s are the distances along the axis from the mirror to the diffuser and the source respectively. When the diffuser is close to the mirror ($z_q/z_s \to 0$) the formula is simpler:

$$\delta = \frac{\lambda R}{2\Delta}.$$

High measurement accuracy is obtained by employing a compensation procedure in which successive transverse and longitudinal (along the axis) shifts of the mirror are made along with a compensating rotation of the mirror in the plane which contains the optical axis and the vector of transverse movement, with the total spatial shift of the mirror equivalent to its rotation with respect to its own center of curvature. In this case local surface nonuniformities

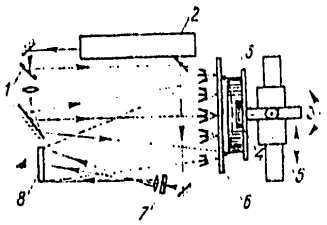

Fig. 1. Diagram of Holographic Shear Interferometer with Diffuser.

Key: 1. Beam splitter
2. LG-38 laser
3. Mirror
4. Etalon
5. Adjutment unit
6. Diffuser
7. Polaroid
8. Hologram

are observed in the same way as in shear interferometers [7], while the radius of curvature is determined from the measured sizes of the movements:

$$R=\frac{\Delta}{\theta},$$

where θ is the angle of the compensating rotation.

Highly accurate measurement of the transverse shift presents no difficulty, since its size is specified in the experiment more or less as desired. The corresponding angles of compensatory rotation are generally very small. Since it is difficult to measure them with a high degree of accuracy, in order to measure the radius of curvature a small diameter standard mirror mounted together with the mirror under test was used.

The difference in radii of curvature results in a difference in the interference patterns observed on the two mirrors after an identical shift of position. This makes it possible to calculate the difference in radii of curvature between the two mirrors without measuring the compensatory angle and increases the accuracy of measurement of the mirror under test.

Measurements were conducted on a series of mirrors with diameters up to 220 mm and with radii of curvature from +10 to -30 meters on a stand about 180 cm long. At the same time these mirrors were tested on an unequal-path Twyman-Green interferometer (aperture 150 mm), measuring their radii of curvature with an autocollimation system. Within the limits of accuracy of measurement on the autocollimation stand (for R = 20 meters the relative error of measurement was 0.5%) no discrepancy between the measurement results was observable.

Fig. 2 shows the interferogram obtained for one of the mirrors in the series (diameter 200 m, radius of curvature -18 m) made for the purpose of measuring local nonuniformities of shape. The measurements were made with tuning to the finite-width fringes [nastroyka na polosy konechnoy shiriny] parallel to the vector of the transverse shift; the shift was 27 mm. A strong deviation of the fringes in the peripheral section of the mirror corresponds to a wave aberration of $\sim$ 0.1 microns measured with the Twyman-Green interferometer.

Thus measurement of the radii of curvature of large mirrors and local nonuniformities on their surfaces by the above method is carried out with a compact device whose dimensions do not depend on the sign and size of the radius of curvature.

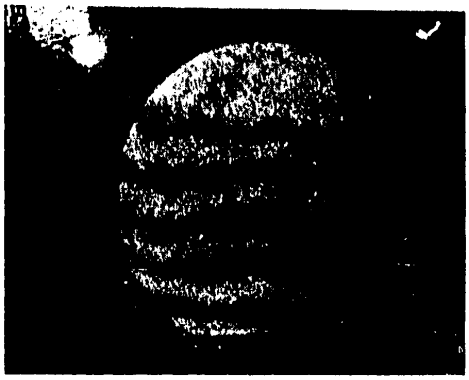

Fig. 3. Shearing Interferogram of a Spherical Mirror with Diameter 200 mm and Radius of Curvature 18,000 mm.

The method is advantageous for testing convex mirrors and small-curvature concave mirrors with radii of curvature ranging from several meters to several dozen meters with a surface reflectivity greater than 20%. The universal method of illuminating all mirrors by a divergent spherical wave from a fixed point source renders the above method suitable for testing of mirrors over an extensive range of diameters. The upper limit on the diameters stems from the requirement for ease of illumination and observation, coherence of the radiation in the mirror aperture and simplicity of interpretation of the interferograms. With source coherent length l, for example, and a distance L between the diffuser and the hologram, it is theoretically possible to conduct measurements on mirrors with diameters up to

$$2L\sqrt{2\frac{l}{L}+\frac{l^2}{L^2}}.$$

With the LG-38 laser used in the experiment, the coherent length of which is $\approx$ 30 cm, and a platform length L $\approx$ 200 cm, it is possible to measure mirrors with diameters up to 220 cm. Mirrors up to 50 cm have been measured in practice. With a laser beam output power of 0.03 W, the delay required to produce the hologram was 100 seconds (a VR-L Mikrat photoplate was used with a radiation wavelength of 0.6328 microns). It would be possible to decrease the exposure time to several seconds by switching to other types of lasers, for example an argon laser with a beam power of 1 W. Using the above method, the measurement of local surface nonuniformities can be carried out with an accuracy approximating that of shearing interferometry. An accuracy of about 0.1 percent was attained in experimental measurements of radii of curvature.

A modification of the apparatus described makes it possible to increase the accuracy of measurement and to expand the range of diameters and radii of curvature of the mirrors that can be tested.

BIBLIOGRAPHY

1. T. T. Dukhopel; and L. G. Fedina. OMP [OPTIKO-MEKHANICHESKAYA PROMYSHLENNOST'], No 8, 1973, p 50.

2. V. A. Savin; and L. G. Fedina. NOVAYA TEKHNIKA V ASTRONOMII, No 3, 1970, p 207.

3. R. Langenbeck. JOSA, Vol 61, No 2, 1971, p 172.

4. V. A. Komissaruk. OMP, No 7, 1969, p 8.

5. R. M. Scott. APPL. OPT., Vol 8, No 3, 1969, p 531.

6. J. Random. US Patent No 3799673, 1974.

7. J. B. Saunders. APPL. OPT., Vol 9, No 7, 1970, p 1620.

Received 12 August 1977.

8480
CSO: 8144/0469

UDC 548.0:535:771.36

AN ELECTROOPTICAL MODULATOR WITH SMALL NONACTIVE LOSSES

Leningrad OPTIKO-MEKHANICHESKAYA PROMYSHLENNOST' in Russian No 9, 1978
pp 71-72

[Article by T. A. Kuzovkova]

[Text] Decreasing non-active losses in the Pockels cells used to modulate light and to control laser generation is a pressing problem of electrooptics. The effort to solve it has stimulated both a search for new types of electro-optical crystals with low absorptivity [1] and the search for new cell designs using short modulating elements.

In some modulators based on the longitudinal Pockels effect in crystals of the KDP and DKDP types [2], the lenght of the modulation element is chosen as 2.5-3 times the diameter. This is because with strip electrodes this is the only way to assure uniform transmission of light in cross section [3].

In order to decrease the length of the modulator element we attempted to concentrate the electrical field in a narrow section of the crystal by using wide tubular electrodes enclosing the lateral surface of the crystal and protruding beyond it for a distance approximately equal to the diameter of the crystal. The gap between the electrodes is chosen with reference to the necessity of maintaining its resistance to breakdown. Here the projecting parts of the electrodes screen the ends of the crystal from effects of the potential in the surrounding space. As a result the electrostatic field is concentrated in a smaller volume than if the electrodes did not project.

The concentration of the field can be strengthened even more if the parts of the electrodes projecting beyond the crystal are galvanically separated from the electrodes on the crystal and given a charge opposite to that of the adjoining electrode.

Fig. 1. presents a cross-sectional diagram of the modulation element with electrodes protruding beyond its end. Fig. 2 illustrates the calculated distribution of residual transmissivity T of the modulator using a KDP crystal and with a length-to-breadth ratio of 1.5.

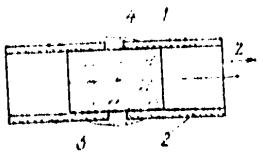

Fig. 1. Electrooptical Modulator

Key: 1. Crystal
2,3. Electrodes
4. High-voltage [dielectric] compound

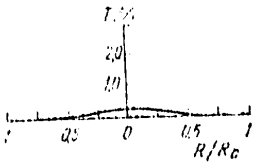

Fig. 2. Transmissivity of Electrooptical Modulator Across Transverse Section of Crystal (Ordinate: Normalized radius R/R_0)

Experimental testing of this modulator indicates that the length of the electrooptical crystal can be decreased to 2/3-1/2 of that in existing designs, and confiems that the projecting parts of the electrodes effectively influence light transmission. With a length-to-breadth ratio of 1.5 for a KDP crystal, for example, and a residual transmissivity through the center of 1% in the off state, the use of protruding electrodes decreased transmissivity by an order of magnitude.

In conclusion we note that when single-polarity voltage pulses are fed to the modulator located inside a grounded screen, the grounded part does not need to be screened from the end of the projecting electrode.

BIBLIOGRAPHY

1. I. S. Rez. In Svoystva materialov, primenyayemykh v ustroystvakh optoelektroniki [Properties of materials employed in optoelectronic devices], USSR Academy of Sciences Corresponding Member K. S. Aleksandrov, ed. Krasnoyarsk, 1975.

2. M. P. Lisitsa. KVANTOVAYA ELEKTRONIKA, No 6, 1972 pp 3-48. Kiev, Naukova Dumka.

3. M. G. Vitkov. OPTIKA I SPEKTROSKOPIYA, Vol 24, No 5, 1968, pp 786-794.

Received 20 July 1977.

8480
CSO: 8144/0469

UDC 539.1.074

AN INFRARED RADIOMETER BASED ON A GALLIUM ARSENIDE INJECTION PHOTODIODE

Leningrad OPTIKO-MEKHANICHESKAYA PROMYSHLENNOST' in Russian No 9, 1978 pp 72-73

[Article by Yu. A. Abramyan, I. D. Anisimova, V. P. Kalyayeva, E. G. Mirzabekyan, I. I. Mikhaylov, R. G. Simonyan and V. I. Stafeyev]

[Text] One method of detecting infrared radiation and measuring its intensity against a background of noise which is several orders of magnitude greater than the signal is a radiometer whose detection range is governed by an input photodetector. In the spectral range of 0.7-0.95 microns, the photodetectors most commonly used for radiometers are gallium arsenide injection photodiodes. We used photodiodes with a pin structure, where the i region is high-resistance gallium arsenide doped with chromium. These photodiodes work with a forward bias, acting as internal amplification photodetectors, and have little noise and an integral sensitivity in the hundreds of milliamperes per lumen.

A schematic of the modulating radiometer developed by us is given in the figure. The radiation is modulated and focused by an optical system on the surface of the gallium arsenide photodetector. An FDK-1 photodiode and an AL107A light-emitting diode, used to produce the reference signal, are located opposite each other on the two sides of the rotating disk. The phases of the reference signal and the signal arriving at the gallium arsenide photodetector are adjusted precisely by shifting the FDK-1 and the AL107A relative to the opening in the radiation modulator. The inner surface of the modulator with the abovementioned components is blackened.

The electrical signal from the photodetector passes to the input of a preamplifier useing a KPZOZYe field transistor. With an input resistance of 10 megohms, the preamplifier noise arriving at the input is 15-17 microvolts. After preamplification and the subsequant amplification stage the signal arrives at the input of a synchronous integrator which acts as a comb filter, its tuning freqeuncy being determined by the reference signal frequency. The synchronous integrator is switched by a square-wave reference voltage obtained by amplifying and shaping the output signal of the FDK-1 and AL107A pair. Silicon transistors in a 1KT011A integrated circuit are used as a key.

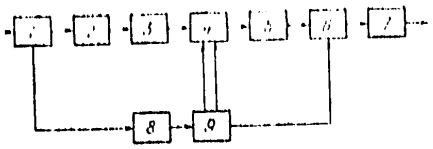

Diagram of IR Radiometer.

Key: 1. IR radiation modulator
2. Low-noise preamplifier
3. First amplification stage
4. Synchronous integrator
5. Second amplification stage
6. Phase detector
7. Matching output stage
8. Reference signal amplifier
9. Reference pulse shaper

Next, after amplification by a K284UD1V operational amplifier with negative feedback for stabilization of the gain, the signal passes through a phase conversion stage and the required emitter repeaters and is fed to the input of a phase detector based on a differential amplifier stage with a current stabilizing transistor (K1UT221B). To trigger the phase detector, a reference voltage is also fed to the K1U221B microcircuit. The utilization of the synchronous detector is justified by its good selectivity and its transmission coefficient greater than 1 [2].

The signal from the output of the phase detector is fed via a differential emitter repeater (a 1NT591A microcircuit) to the output for recording by a KSP-4 recorder with a 10-microvolt full-scale deflection. The radiometer time constant is 2-3 seconds. The threshold sensitivity in recording is $1.5 \cdot 10^{-15}$ W-Hz$^{-1/2}$ (using a photodiode cooled to 77° K). The threshold sensitivity of the radiometer with an uncooled photodiode is $3 \cdot 10^{-13}$ W-Hz$^{-1/2}$. An LED with a wavelength of 0.8 microns was used as the radiation source.

The use of recently-developed injection diodes with a threshold sensitivity of $5 \cdot 10^{-16}$ W-Hz$^{-1/2}$ (at 77° K) in the radiometer will improve its threshold sensitivity.

BIBLIOGRAPHY

1. A. V. Ipatov; and A. B. Berlin. IZVESTIYA VUZOV, Vol, 16, No 5, 1973.

2. M. S. Reytman; and Yu. N. Rybin. Elektronnaya tekhnika v avtomatike [Electronic Equipment in Automatic Control]. Yu. Konev, ed. No 4, 1973, p 79.

Received 20 July 1977.

8480
CSO: 8144/0469

END